Ryanodine Receptor Calcium Release Channels in Trophoblasts and their Role in Cell Migration

Limian Zheng[a], Andrew Lindsay[b], Kate McSweeney[a] , John Aplin[c], Karen Forbes[c,d], Samantha Smith[c], Richard Tunwell[e], John James Mackrill[a]

Abbreviated institutional affiliations: [a]Department of Physiology, and [b]School of Biochemistry and Cell Biology, University College Cork, Ireland; [b]Maternal and Fetal Health Research Centre, University of Manchester, UK; [c]Leeds Centre for Reproduction and Early Development, University of Leeds, UK; and Division of Biosciences, University College London, Gower Street, London, UK.

Corresponding author: John James Mackrill, Department of Physiology, School of Medicine, University College Cork, Western Gateway Building, Western Road, Cork, Ireland. T12 XF62. Tel: +353 (0)21 4901400. Fax: +353 (0)21 4205370. Email: j.mackrill@ucc.ie; Web URL: http://publish.ucc.ie/researchprofiles/C008/jmackrill.

Abbreviations: AM, acetoxymethyl ester; AGII, angiotensin II (AGII); AT1, AGII type 1 (receptor); AVP, arginine vasopressin; CICR, Ca^{2+}-induced Ca^{2+}-release; CASQ, calsequestrin; DMSO, dimethyl sulfoxide; ER, endoplasmic reticulum; ET1, endothelin type 1 (receptor) KHB, Krebs-Henseleit Bicarbonate buffer; IHC, immunohistochemistry; IP_3R, inositol 1,4,5-trisphosphate receptor; PE, pre-eclampsia; Ry, ryanodine; RyR, ryanodine receptor; PBS, phosphate buffered saline; PLC, phospholipase C; PVDF, polyvinylidene difluoride; SR, sarcoplasmic reticulum; Tet, tetracaine; TRDN, triadin.

Abstract

Trophoblasts are specialized epithelial cells of the placenta that are involved in invasion, communication and the exchange of materials between the mother and fetus. Cytoplasmic Ca^{2+} ($[Ca^{2+}]_c$) plays critical roles in regulating such processes in other cell types, but relatively little is known about the mechanisms that control this second messenger in trophoblasts. In the current study, the presence of RyRs and their accessory proteins in placental tissues and in the BeWo choriocarcinoma, a model trophoblast cell-line, were examined using immunohistochemistry and Western immunoblotting. Contributions of RyRs to Ca^{2+} signalling and to random migration in BeWo cells were investigated using fura-2 fluorescent and brightfield videomicroscopy. The effect of RyR inhibition on reorganization of the F-actin cytoskeleton elicited by the hormone angiotensin II, was determined using phalloidin-labelling and confocal microscopy. RyR1 and RyR3 proteins were detected in trophoblasts of human first trimester and term placental villi, along with the accessory proteins triadin and calsequestrin. Similarly, RyR1, RyR3, triadin and calsequestrin were detected in BeWo cells. In this cell-line, activation of RyRs with micromolar ryanodine increased $[Ca^{2+}]_c$, whereas pharmacological inhibition of these channels reduced Ca^{2+} transients elicited by the peptide hormones angiotensin II, arginine vasopressin and endothelin 1. Angiotensin II increased the velocity, total distance and Euclidean distance of random migration by BeWo cells and these effects were significantly reduced by tetracaine and by inhibitory concentrations of ryanodine. RyRs contribute to reorganization of the F-actin cytoskeleton elicited by angiotensin II, since inhibition of these channels restores the parallelness of these structures to control levels. These findings demonstrate that trophoblasts contain a suite of proteins similar to those in other cell types possessing highly developed Ca^{2+} signal transduction systems, such as skeletal muscle. They also indicate that these channels regulate the migration of trophoblast cells, a process that plays a key role in development of the placenta.

Keywords: trophoblast, placenta, ryanodine receptor, calcium signalling, cell migration

1. Introduction

The placenta is a unique organ in mammals, that provides an interface for communication and the transport of nutrients and waste products between mother and fetus [1]. Trophoblasts are epithelial cells of the placenta that are crucial for performing these activities Within villi of the human placenta, cytotrophoblasts proliferate, migrate and fuse to form a multinucleate structure called the syncytiotrophoblast. In addition, extravillous trophoblasts are involved in invasion of the maternal tissues. Trophoblasts play an essential role in mineralization of the fetal skeleton, participating in transcellular transport of Ca^{2+}[2]. Abundant Ca^{2+} channels, Ca^{2+} pumps and Ca^{2+} binding proteins found in trophoblasts are likely to fulfil such transport roles [3]. Furthermore, disturbances in Ca^{2+} transport processes are considered to participate in pregnancy-related diseases such as pre-eclampsia (PE) and intrauterine growth restriction [4].

In addition to its critical function in formation of the skeleton, Ca^{2+} is a key second messenger in cellular organisms, regulating processes ranging from gene expression, to motility, to cell-death [5]. Ryanodine receptors (RyRs) are a family of high-conductance channel proteins that release Ca^{2+} from intracellular stores, such as the sarcoplasmic and endoplasmic reticulum (SR/ER) [6]. Pharmacologically, RyRs are characterized by being modified by the plant-derived toxin ryanodine: this alkaloid gates RyRs at nanomolar concentrations, but antagonizes these channels at concentrations above 10 μM [7]. In mammals, there are three RyR types encoded by distinct genes, whose protein products display differential but overlapping tissue distributions [8], [9]. RyR1 is highly abundant in the triad junctions of skeletal muscle, formed between two terminal cisternae of the SR abutting the T-tubular infoldings of the sarcolemma (muscle cell-surface membrane). At these triad junctions, RyR1 is gated by allosteric interactions with a sarcolemmal voltage-sensor called $Ca_v1.1$, thereby coupling action potentials to Ca^{2+} release from the SR and subsequent activation of the contractile apparatus. Transgenic mice lacking the *RYR1* gene die perinatally from asphyxia, as a consequence of defective excitation-contraction coupling in the respiratory muscles [10]. RyR2 is found at greatest levels in the heart, where it is gated by the influx of Ca^{2+} via a distinct voltage-gated Ca^{2+} channel, $Ca_v1.2$, in a process termed Ca^{2+}-induced Ca^{2+}-release (CICR) [11] . Transgenic mice with disrupted *RYR2* die *in utero* at approximately *post-coitum* day 10, associated with morphological defects of the heart tube [12]. RyR3 displays a wide, low-abundance tissue distribution with highest amounts in brain and smooth muscle. *RYR3-/-*

transgenic mice are viable and fertile, but display subtle behavioural deficits, indicating roles in the central nervous system [13].

RyR channels are formed from tetrameric assemblies of very high molecular weight protein subunits, each of which is in the order of 550 kDa. These complexes are associated with a wide range of accessory proteins that modulate the function of these channels in a cell-specific manner [7]. Such accessory proteins include kinases, phosphatases, Ca^{2+}-binding proteins, prolyl isomerases and molecular scaffolds. For example, calsequestrins (CASQ1 and CASQ2) are high-capacity SR lumenal buffering proteins that also regulate RyR gating in response in the degree of SR Ca^{2+} loading [14]. Triadin (TRDN) is a single transmembrane spanning protein that is highly enriched in the triad junctional SR of skeletal muscle, where it anchors CASQs to RyR1. Multiple isoforms of TRDN are generated by alternate splicing of its mRNA in a tissue-specific manner, generating proteins that have functions in addition to linking RyRs to CASQs [15].

Although RyRs and their accessory proteins have been detected in a wide range of cell types [8], [9], their roles have only been extensively characterized in striated muscle excitation-contraction coupling and in vascular smooth muscle relaxation. Cytosolic Ca^{2+} plays key roles in controlling cell migration and several lines of evidence indicate a role for RyR-mediated Ca^{2+} release in this process [16]. In murine astrocytes, pharmacological inhibition or genetic ablation of RyR3 results in decreased random migration, but does not significantly alter chemotaxis [17]. In human nasopharyngeal carcinoma cells, Ca^{2+} influx through transient receptor potential melastatin 7 (TRPM7) cation channels leads to opening of RyRs via CICR: inhibition of any of these steps decreases migration [18, p. 7]. It is postulated that the cytotoxicity and decreased random migration of human melanoma cells elicited by Euplotin C, a secondary metabolite of the marine ciliate *Euplotes crassus*, are consequences of it gating RyRs [19].

Trophoblast migration into maternal tissues is crucial for formation of the placenta [1]. Changes in cytosolic Ca^{2+} concentration ($[Ca^{2+}]_c$) are known to regulate this process. Receptors for several hormones are potentially coupled to Ca^{2+} signalling in trophoblasts. For example, angiotensin II (AGII) type 1 (AT1R) and *Mas* receptors (*Mas*R) are expressed in human placenta, where they control hormone secretion, trophoblast invasion and vasoregulation [20], [21]. The pituitary gland peptide arginine vasopressin (AVP) plays important roles not only in vasoconstriction and water re-absorption in the collecting ducts of the kidney, but also in the regulation of amniotic fluid volume and composition [22]. ET1 is the predominant isoform of endothelin peptide in the placenta, which stimulates trophoblast differentiation, proliferation,

cell invasion and cell-death through activation of ET-A and ET-B receptors [23]–[25]. These different receptors all initiate increases in $[Ca^{2+}]_c$ by activating phospholipase C (PLC), generating the second messenger inositol 1,4,5-trisphosphate (IP_3) and stimulating Ca^{2+} release from the ER via IP_3R channels, which belong to the same channel superfamily as RyRs. Although IP_3-mediated Ca^{2+} release is amplified by CICR in other cell types [5], the participation of RyRs in such pathways has not been demonstrated in trophoblasts. Alternatively, in other cell types, RyRs might be gated by CICR, or by allosteric coupling operating through voltage-gated Ca^{2+} channels. For example, RyR1 is a minor subtype present in rat brain, but unlike the major RyR2 form, is co-immunoprecipitated by antibodies recognizing the voltage-gated Ca^{2+} channels $Ca_v1.2$ and $Ca_v1.3$ [26].

Expression of mRNAs encoding all three RyR types has been reported in human term placenta and has shown to be significantly decreased in subjects diagnosed with PE. Although these observations suggest that RyRs plays physiological roles in the placenta, the particular cell types in which they are expressed have not been determined and their contributions to Ca^{2+} signalling have not been directly investigated. Consequently, the current study aimed to: 1) identify the RyRs and accessory proteins present in human placental trophoblasts and in the trophoblastic cell-line BeWo; 2) examine the roles of BeWo cell RyRs in the $[Ca^{2+}]_c$ transients evoked by endogenously occurring hormones AGII, AVP, or ET1; and 3) to investigate the effects of antagonistic concentrations of ryanodine on the random migration of the BeWo choriocarcinoma, and the organization of F-actin within these cells.

2. Materials and Methods

2.1 Materials

Cell culture media were obtained from Sigma-Aldrich (Poole, UK). General laboratory chemicals of analytical reagent grade or better were obtained from Sigma-Aldrich or Calbiochem-Novabiochem Ltd. (Nottingham, UK). Antibodies from commercial sources were used at the following dilutions: rabbit anti-RyR1 (Millipore #AB9078A, 1:1000 for Western blot, 1:500 for immunohistochemical staining (IHC)); rabbit anti-RyR2 (Sigma-Aldrich #HPA016697, 1:250 for Western blot, 1:25 for IHC); rabbit anti-RyR3 (Millipore # AB9082, 1:1000 for Western blot, 1:500 for IHC); mouse monoclonal anti-TRDN (Pierce #MA3-927 (mAb GE 4.90), 1:100 for both Western blot and IHC); rabbit anti-CASQ (Pierce #PA1-913, 1:100 for Western blot); and mouse anti-cytokeratin-7 (Dako #M7018 (mAb OV-TL 12/30),

1:500 for IHC). A rabbit anti-pan RyR antiserum (RS4, 1:500 dilution for Western blot) against a synthetic peptide of sequence SFPNNYWDKFVKRKV, corresponding to residues 4639-4653 of human RyR2 and sharing 100% and 93% identity with *Homo sapiens* RyR3 or RyR1, was produced essentially as described previously [9]. A rabbit polyclonal antibody (pAb 69, 1:500 dilution on Western blot) was prepared against a fusion protein from the N-terminal 121 amino acid residues of the voltage-gated Ca^{2+} channel, $Ca_V1.3$. This fusion protein shares extensive sequence identity with the corresponding region of $Ca_V1.2$ and the resulting antibodies cross-react with this protein [26]. The human BeWo, JEG-3, A549, SH-SY5Y and MDA-MB-231 cell-lines were originally obtained from, and cultured according to the protocols of, the European Collection of Animal Cell Cultures (Salisbury, UK). Uncoated glass-bottom microscope dishes (35 mm diameter, 10 mm diameter coverslips, 0 thickness) were from MatTek Corporation (Oregon, USA). Fura-2 acetoxymethyl (AM) ester from Invitrogen was purchased from BioSciences Ireland (Dun Laoghaire, Co. Dublin, Ireland).

2.2 Human tissues and ethical considerations

All immunohistochemistry involving human placental tissues was performed at the Maternal and Fetal Health Research Lab, St. Mary's Hospital, Manchester under approval of the Central Manchester Local Ethics Committee. Villous tissue homogenates of both human first and term placenta were prepared by Maternal and Fetal Health Research Group, University of Manchester, as described previously [27]. Normal late first trimester placentas were obtained, following maternal informed consent and approval from Manchester Local Research Ethics committee at elective surgical or medical termination of pregnancy and were dissected as described previously [27]. Additional samples of human term placental villous tissues were obtained from Dr. Moore Department of Biochemistry, University College Cork, as approved by the Clinical Research Ethics Committee of the Cork Teaching Hospitals, following maternal informed consent. Homogenates or microsomal membranes were prepared from rat tissues (male Sprague-Dawley, 8 to 10 weeks old, from the Biological Service Unit of University College Cork) as positive controls, essentially as described previously [9].

2.3 Cell culture

Human BeWo trophoblast cells were maintained in Nutrient Mixture F12 Ham medium, supplemented with 2 mM L-glutamate, 50 IU/ml of penicillin, 50 μg/ml of streptomycin, and 10% (v/v) heat-inactivated fetal bovine serum [28]. Cells were maintained in a humidified

atmosphere of 95% air and 5% CO_2 at 37°C. They were subcultured every three days using trypsin-EDTA and were plated at a density of 40,000 cells/cm^2.

2.4 Preparation of microsomes and membrane subfractions

All steps were performed at 0 to 4°C. All buffers contained protease inhibitors (2 mM benzamidine, 2 μg/ml aprotinin, 2 μg/ml leupeptin, 2 μg/ml pepstatin A, and 0.5 mM PMSF). Crude microsomal membranes from rabbit or rat tissues, or from the BeWo cell-line, were prepared as described previously [9]. Human term placental villous tissue homogenates were prepared in 1.5 ml Eppendorf tubes, with tissue (50-100 mg wet weight) being homogenized in ice-cold 0.25M sucrose, 10 mM Tris pH7.4 (500 μL) and protease inhibitors using pellet pestles. Crude homogenates were centrifuged at 1,100 x *g* for 10 min (Rotor F45-30-11, Eppendorf Centrifuge 5810R; Eppendorf UK Ltd.). The resulting supernatants were further centrifuged at 7,700 x *g* for 20 min. Microsomal membranes were collected from these supernatants by centrifugation at 30,000 x g for 60 min. Microsomes were resuspended in 5 volumes/pellet volume of 0.25M sucrose, 10 mM Tris pH7.4 and protease inhibitors by passage through a 25 G needle, then were stored at -80°C until use. Protein concentrations of the microsomes obtained were determined using the Bradford protein assay, with bovine serum albumin as a standard.

2.5 SDS/PAGE and immunoblotting

Membrane proteins were resolved on 7% or 5% (w/v) reducing SDS-PAGE mini-gels and then were transferred to polyvinylidene difluoride (PVDF) membranes. The transfer buffer consisted of 20 mM Tris base, 150 mM glycine and 0.037% (w/v) SDS. Note that omission of methanol from the transfer buffer is critical for efficient transfer of very high molecular weight proteins, such as RyRs. These were transferred using a BioRad minigel wet blotter at 70V constant voltage for 2 h (1 h for all other proteins). Blots were blocked with 5% (w/v) milk-PBS for 1 h before overnight incubation at 4°C with antisera, diluted in the same blocking buffer. Membranes were washed three times in PBS for 15 min, then were incubated with a 1:500 dilution of horseradish peroxidase-conjugated anti-mouse IgG or a 1:2000 dilution of horseradish peroxidase-conjugated anti-rabbit IgG in milk-PBS for 1 h. Blots were washed three times in PBS for 45 min. Immunoreactive proteins were detected by using enhanced chemiluminescence kit (Pierce ECL Western Blotting Substrate, Thermo Scientific, Fisher Scientific Ireland), and visualized on Kodak X-Omat LS film using AGFA CP1000 developer, according to the manufacturers' instructions.

2.6 Immunohistochemistry

For immunohistochemistry (IHC), human placental villous tissue was prepared, embedded in paraffin, then sectioned (5 μm) and mounted on glass slides, as described previously [27]. Samples in sections were treated with primary antibodies (rabbit polyclonal anti-RyR1 (1:500), Millipore; rabbit polyclonal anti-RyR2 (1:25), Sigma; rabbit polyclonal anti-RyR3 (1:500), Millipore; monoclonal mouse anti-triadin (1:100, clone GE4.90, Pierce), followed by the avidin-peroxidase detection method [27]. Stained sections were visualized by Leitz Dialux 22 microscope, using Phaco 100x/1.20 NA water objective; images were captured using a QI Cam Fast 1394 camera and analyzed by Image Proplus 6.0 imaging system.

2.7 Fura-2 fluorescence microscopy

BeWo cells were grown to approximately 10,000 cells/cm^2 on 35 mm glass bottom dishes; and were incubated with 5 μM fura-2 AM and 5 μM Pluronic F-127 (BioSciences Ireland) in sterile-filtered modified Krebs-Henseleit Bicarbonate (KHB) buffer (NaCl 120 mM, KCl 4.8 mM, $MgSO_4$ 1.2 mM, KH_2PO_4 1.2 mM, $NaHCO_3$ 25 mM, $CaCl_2$ 2 mM, glucose 10 mM, HEPES 5 mM, pH 7.2) for 45 min at 37°C. Fura-2-loaded cells were placed on the stage of an Olympus IX51 inverted fluorescence microscope (Olympus Optical Co. (UK) Ltd.). Images were captured using a Hamamatsu ORCA-ER Digital Camera C4742-80 and processed using Andor IQ acquisition software version 2.0 (Andor Technology Ltd. Belfast, Northern Ireland), with alternating illumination at 340 and 380 nm for excitation; pairs of fluorescence images were obtained every 800 ms through an objective lens (Olympus UPlanFI100XOI3 oil-immersion objective 100x/1.3NA) and a dichroic emission filter (470-550 nm). Time-related changes in $[Ca^{2+}]_c$ of single cells were expressed as changes in mean fura-2 ratio within defined regions-of-interest; only cells whose initial resting ratios in the range 0.4-0.8 were used for analysis [29]. To indirectly estimate ER Ca^{2+} content, the magnitude of thapsigargin (TG)-induced Ca^{2+} release was monitored for 10 min using fura-2 and the area-under-the-curve (a.u.c) of this response was determined. TG is a plant-derived tumour-promoter which inhibits SR/ER-Ca^{2+}-ATPase (SERCA) pumps, thereby unmasking Ca^{2+} leak pathways in these organelles [30], [31].

2.8 Analysis of Random Cell Migration

Cells were subcultured at a density of 5,000 cells/cm^2 on 35 mm sterile plastic dishes, in 1 mL of culture medium supplemented with 10 mM HEPES. A day later, additions of 200 nM AGII in the presence or absence of 100 μM ryanodine were made, then cells were imaged with brightfield illumination every 5 min for 8 h, at 37°C, using an Olympus IX51 microscope (10x, 0.3 N.A. objective; Hamamatsu ORCA ER CCD videocamera). Videos were exported as multi-dimensional TIFF files and cell migration paths were plotted using the Manual Tracking plugin of ImageJ (https://imagej.nih.gov/ij/plugins/track/Manual%20Tracking%20plugin.pdf). Cell migration paths were exported to the Chemotaxis and Migration Tool from Ibidi (https://ibidi.com/img/cms/products/software/chemotaxis_tool/IN_XXXXX_CT_Tool_2_0.pdf). This allowed estimation of the velocity, total distance travelled, Euclidean distance travelled (length of the straight line from origin to end point) and directionality ("how straight" the path was, with "0" being a random path and "1" being a straight line) for each cell [32].

2.9 Quantification of F-actin organization by phalloidin staining

Cells seeded on 10 mm glass coverslips were treated with vehicle, 200 nM AGII, 100 μM Ry, or 200 nM AGII plus 100 μM Ry for 2 h and subsequently fixed with 4% paraformaldehyde, quenched with 50 mM NH4Cl, and permeabilized in 0.1% TX-100/phosphate-buffered saline (PBS) for 5 min at room temperature, and blocked with 5% FBS/PBS for 30 min. Cells were labelled with Texas Red-phalloidin (ThermoFisher, 1:1000 dilution) and DAPI (1:20000 dilution) in 5% FBS/PBS for 1 h at room temperature. Coverslips were washed extensively with PBS and mounted on glass slides using Mowiol. Images were acquired on a Zeiss LSM510 confocal microscope using 64X 1.4 NA objective (Carl Zeiss, Jena, Germany). All acquisition settings were kept the same for all treatment conditions within an experiment.

Images were exported as TIFF files and were analysed using the LPX plugin on ImageJ, essentially as described by Higaki [33] and illustrated in Fig. 8A. In brief, the Texas Red channel of each merged image was extracted and regions of interest (ROIs) drawn around each cell. F-actin phalloidin-stained images were skeletonized and numerical parameters were extracted from each cell "skeleton". These values were: the area of the cell; orientation relative to the x-axis of the field of view; average angle of the cytoskeleton relative to the long-axis of the cell; the overall length of the actin cytoskeleton; the density of the cytoskeleton; bundling, a measure of the grouping of F-actin; and parallelness, a parameter indicating how aligned the F-actin fibres are relative to each other, with a value of 1 indicating that all fibres are parallel.

2.9 Statistics

Mean values (±standard error in the mean, SEM) were compared using an unpaired student's t-test, with p values of < 0.05 taken as significant. Where more than two mean values were compared, data were analysed using one-way ANOVA followed by Tukey's Multiple Comparison Test with GraphPad Prism 4.0 software, taking p values of <0.05 as significant. For fura-2 calcium and cell migration assays, the number of experiments performed, 'n', refers to the number of dishes used rather than the number of individual cells assayed in each dish.

3. Results

3.1. RyRs and their accessory proteins in human trophoblastic tissues

To determine if RyR proteins are present in human trophoblastic tissues, sections of villi from first trimester and term placentas were probed with subtype-selective antibodies by IHC microscopy. These investigations revealed that RyR1 (*Fig. 1A, panels I. and II.*) and RyR3 (*Fig. 1A, panels V. and VI.*) are abundant in the outermost two layers of villi from both first trimester and term tissues. The innermost of these layers is composed of cytotrophoblasts (*arrows*) and outer of syncytiotrophoblasts (*asterisks*), as confirmed by robust staining of these cells with antibodies recognising cytokeratin-7 (*Fig. 1A, panels VII. and VIII.*), a characteristic marker of the trophoblastic lineage [34]. In all of these images, the positive immunostaining observed was specific, since it was not detected in the absence of primary antibodies (*Fig. 1A, 'Null', panels IX. and X.*). RyR2 was not detectable in either term or first trimester villi (*Fig. 1A, panels III. and IV.*). This was not a result of the anti-RyR2 antibody used being unsuitable for this technique, since it strongly labelled various cell types present in first trimester decidual bed tissue (*Fig. 2A*), under identical conditions. These cell types were not detectably stained in the absence of primary antibody (*Fig. 2B*), including those that were labelled with anti-cytokeratin-7 antibodies (*Fig. 2C*).

Gating of RyR Ca^{2+} channels is regulated by interactions with a range of accessory proteins. Of these, triadin (TRDN) serves as a linker communicating between RyRs and calsequestrins (CASQ), high capacity SR/ER lumenal Ca^{2+} storage proteins [7]. In first trimester and term placental villi, both cytotrophoblasts (*arrows*) and syncytiotrophoblasts (*asterisks*) were specifically labelled with an antibody recognising the C-terminal 34 residues of TRDN [35] (*Fig. 1B, panels I and II*). On Western blots, TRDN was detected as a band of approximately 95 kDa apparent molecular weight in homogenates from term placental villi (*Fig. 1C i)*). Attempts to use a rabbit anti-CASQ polyclonal antibody for IHC of villous samples were unsuccessful. However, this antibody detected a doublet of 50 to 60 kDa apparent

molecular weight in term placental villous homogenates, corresponding to products of the *CASQ2* and *CASQ1* genes (*Fig. 1C ii)*). The higher molecular weight proteins (>100 kDa) detected on immunoblots probed with anti-CASQ antibodies probably represent CASQ-like proteins, which have previously been reported in both skeletal and cardiac muscle [36]. The molecular identity of these CASQ-like proteins is unknown. They persist under reducing, denaturing SDS-PAGE conditions; cross-react with multiple anti-CASQ antibodies; but their abundance is selectively decreased in skeletal muscle from *mdx* dystrophic mice, with no apparent change in the levels of monomeric CASQ [37].

3.2. RyRs and their accessory proteins in the BeWo choriocarcinoma

RyRs and their accessory proteins were also detected in the BeWo choriocarcinoma, a model trophoblastic cell-line [1], [28]. In Western immunoblot assays, a custom-made anti-pan RyR antiserum, RS4, recognized proteins of >500 kDa apparent molecular weight in rat heart, rat skeletal muscle and in microsomal membranes prepared from BeWo. It is likely that these proteins correspond to RyR1 and RyR3, since antibodies directed against these channel proteins detected >500 kDa bands in the BeWo cell-line and positive controls, although not in negative control tissues or cell-lines. RyR2 protein was only detected in rat heart and not in BeWo, rat skeletal muscle or rat brain, (*Fig. 3A)*. RyR accessory proteins were also present in the BeWo choriocarcinoma: the 95 kDa spliceform of TRDN; the 50 and 60 kDa forms of CASQ; and proteins of approximately 220 kDa detected by a polyclonal antibody against the Cav1.2/1.3 members of the voltage-gated Ca^{2+} channel family, (*Fig. 3B)*.

3.3. Ryanodine increases cytoplasmic [Ca^{2+}] in BeWo cells

The neural alkaloid ryanodine (Ry) binds to RyRs by a negative allosteric mechanism, activating the channel at low concentrations (1 nM-1μM) by increasing its open probability. Higher concentrations of Ry (above 10 μM) inactivate the channel by promoting a closed conformation [7]. Within 5 min of addition, 1 μM Ry caused a significant rise in fura-2 ratio that reached a peak of 0.24 ± 0.03 (n = 11) above a resting ratio of 0.54 ± 0.02 (*Fig. 4A, $p <$ 0.001 Ry versus vehicle*) in BeWo cells, equivalent to a 44 ± 6 % increase over the basal level. To test the specificity of this Ry-induced Ca^{2+} rise, the antagonist tetracaine (Tet) was used. Tet is a local anaesthetic, which inhibits RyR-mediated Ca^{2+} release in skeletal and cardiac muscles [38]. Pre-incubation of BeWo cells with 100 μM Tet resulted in a significant suppression of the Ry-induced rise in fura-2 ratio (*Fig. 4B and C: $p< 0.01$, Ry versus Ry plus*

Tet). The change in mean fura-2 ratio was 0.15 ± 0.03 (n = 8) over basal level (0.57 ± 0.03), corresponding to a 30 ± 7 % increase above the resting value (*Fig. 4B.*). This suppression by Tet showed two phases: an initial inhibition during which cells showed responses similar to those caused by the vehicle alone, followed by a gradual rise in fura-2 ratio, whose peak was smaller than that in cells stimulated with 1 μM ryanodine alone. Dantrolene is a hydantion derivative that is a selective antagonist of RyRs [7]. Attempts to use this antagonist to inhibit Ca^{2+} increases stimulated by 1 μM Ry in Bewo cells were unsuccessful, since this reagent caused a rise in cellular autofluorescence at an excitation wavelength of 380 nm (even in the absence of fura-2), leading to an artefactual decrease in fura-2 ratio, (*Supplemental Fig. 1A).* The artefactual decrease in fura-2 ratio caused by dantrolene was first reported in bullfrog sympathetic neurones [39], but has not been consistently observed in all cell types tested (*JJM, unpublished observations*), suggesting that it is dependent on the presence of specific cellular components.

3.4. Ryanodine-sensitive channels contribute to $[Ca^{2+}]_c$ elevations elicited by peptide hormones in BeWo cells.

In BeWo cells, application of 200 nM AGII [20], 200 nM AVP [22] or 1 nM ET1 [24], [29] evoked significant increases in mean fura-2 ratio (over the basal ratio) of 74 ± 15 % (n = 9), 33 ± 11 % (n = 6), and 44 ± 9 % (n = 6) above the resting level. The specificity of these rises in fura-2 was demonstrated by the use of pharmacological inhibitors, each of which significantly reduced responses to the corresponding peptide hormone: 5 μM A779, a *Mas*R selective inhibitor; 5 μM losartan, AT1 receptor selective antagonist; 100 nM SR49059, a V1a receptor selective antagonist; or 100 nM BQ123, an ET_A receptor selective antagonist, (*Fig. 5).* These antagonists were added 5 min prior to the addition of the corresponding hormone and were present throughout the remaining time.

These observations demonstrate that activation of AT1, *Mas*, V1a, or ET_A receptors is coupled to $[Ca^{2+}]_c$ elevations in BeWo cells during stimulation by AGII, AVP or ET1, presumably by activation of PLC, production of IP_3 and stimulation of Ca^{2+} release via IP_3Rs. All three types of IP_3R have been detected at the mRNA level in human placenta [4] and endothelin triggers ER stress in BeWo cells via activation of the PLC-IP_3-IP_3R-Ca^{2+} release pathway [29]. Attempts to dissect this pathway further were unsuccessful, since both the PLC inhibitor U73122 and the IP_3R antagonist 2-aminoethoxydiphenyl borate caused increases in fura-2 ratio in BeWo cells in their own right (*Supplemental Fig.1Band C*).

To determine whether RyR-mediated Ca^{2+}release from internal stores contributed to hormone-induced rises in $[Ca^{2+}]_c$ in the BeWo choriocarcinoma, cells were pre-incubated with the RyR antagonists Tet or Ry for 5 minutes before application of AGII, AVP or ET1 (*Fig. 5*). Tet or Ry were also present for the remaining time. Tet or Ry (100 μM) significantly suppressed the AGII, AVP or ET1-induced rises in fura-2 ratio in BeWo cells, with the traces from cells treated with these antagonists resembling those treated with vehicle alone. These observations indicate that RyR-mediated Ca^{2+} release makes a major contribution to the elevations in $[Ca^{2+}]_c$ in BeWo cells upon stimulation by AGII, AVP or ET1.

A possible explanation for the effects of 100 μM Ry on hormone-elicited increases in $[Ca^{2+}]_c$ in BeWo cells is that it causes sustained activation of these channels, thereby depleting the Ca^{2+} stores, rendering them refractory to Ca^{2+} release triggered by other pathways, such as the IP_3Rs [31]. To test this possibility, cells were treated with the SR/ER Ca^{2+}-ATPase inhibitor thapsigargin (TG) [30], in order to gauge the magnitude of Ca^{2+} store loading. Pre-treatment of BeWo cells with 100 μM Ry for 5 minutes significantly decreased the resting fura-2 ratio, relative to those exposed to vehicle or 100 μM Tet, *Fig. 6B*. However, in 100 μM Ry-treated cells TG causedfura-2 responses which were of reduced magnitude compared with those subjected to vehicle or 100 μM Tet, but this difference was not statistically significant, *Fig. 6A and 6C*. In subsequent experiments, the effects of RyR antagonists on BeWo cell migration were monitored for up to 8 hours. Following 8 hours of incubation, neither 100 μM Tet nor 100 μM Ry significantly altered the magnitude (AUC) of the TG-induced rise in fura-2 ratio in BeWo cells relative to the vehicle control, *Fig. 6C*. These observations are consistent with 100 μM Ry inhibiting RyRs, rather than activating these channels.

3.5. Ryanodine-sensitive channels contribute to migration of BeWo cells in response to angiotensin II.

In order to determine the effects of RyRs on BeWo random migration, cells were stimulated with AGII in the presence or absence of antagonists of these channels and were tracked for 8 hours using brightfield videomicroscopy. On its own, AGII increased BeWo velocity (*Fig. 7C*), accumulated distance (*Fig. 7D*), Euclidean distance (*Fig. 7E*) and directionality (*Fig. 7F*) of random migration, compared with the vehicle-only control. Co-addition of an inhibitory concentration of Ry (100 μM) altered the random migration of AGII-treated cells (*Supplemental video 1; Fig 7A and B*), ablating the effects on velocity, accumulated distance and Euclidean distance travelled, but not those on directionality. Inhibition of RyRs also

abolished the increase in velocity of random migration triggered by AGII in the JEG-3 human trophoblastic cell-line, (*Supplemental Fig. 2*).

The effects of other Ca^{2+}-modulating small molecules on BeWo random migration were also assessed. The SR/ER Ca^{2+} ATPase inhibitor thapsigargin (500 nM), and the RyR antagonists Tet (100 μM) and dantrolene (50 μM), all increased BeWo velocity, accumulated distance, Euclidean distance and directionality relative to vehicle-treated cells. In contrast, an activating concentration of Ry (1 μM) only increased directionality, but did not significantly alter the other parameters, *Supplemental Fig. 3*. Thapsigargin and tetracaine exerted significant cytotoxicity on BeWo cells (as assessed by trypan blue staining) within a period of 2 hours. To circumvent this problem, the effects of 100 μM Tet on random and AGII stimulated migration were assessed for a period of 2 hours. Like Ry, 100 μM Tet significantly inhibited AGII stimulated increases in cell velocity (Fig. 7G) and consequently, on accumulated distance travelled (Fig. 7H). However, unlike Ry, Tet had no significant effect on Euclidean distance travelled, nor on directionality.

To investigate the molecular mechanism by which RyRs contribute to the effects of AGII on BeWo migration, the organization of the F-actin cytoskeleton was examined [40]. Efforts to introduce a plasmid encoding fluorescent peptide-based probe, LifeAct-mCherry, into BeWo cells to dynamically image F-actin organization [41], were unsuccessful due to low transfection efficiency. Subsequently, cells were stained with a Texas Red conjugate of phalloidin [42], a fungal bicyclic heptapeptide which selectively binds to F-actin. Analysis of confocal micrographs of BeWo cells stained with this probe revealed that AGII significantly decreased F-actin parallelness and that this effect was abolished by co-addition of a inhibitory concentrations of either Ry or Tet (100 μM), *Fig. 8*.

5. Discussion

RyRs are high conductance calcium release channels known to regulate specialized physiological processes in a restricted range of cell types. These include excitation-contraction coupling in striated muscles, relaxation of smooth muscles, water transport in collecting duct epithelia and synaptic plasticity in the brain [43]. A report indicating the presence of mRNAs encoding all three RyRs in placenta and downregulation of these in PE [4] prompted the current investigation into the presence of these channels and their accessory proteins in trophoblasts. Using IHC microscopy assays, both cytotrophoblasts and syncytiotrophoblasts from first trimester and term placental villi were found to express both RyR1 and RyR3 but did not

display detectable levels of RyR2. The expression of RyR1 and RyR3 is reminiscent of that in skeletal muscle, in which the former subtype plays an essential role in coupling membrane depolarization to Ca^{2+} release. Similarly, the BeWo human choriocarcinoma was shown to contain RyR1 and RyR3 proteins.

CASQ and TRDN were also present in trophoblasts of placental villi and within the BeWo cell-line. CASQ acts as a high-capacity, low-affinity calcium storage protein that is only abundant in striated muscles and possibly in cerebellar Purkinje neurons [7], [44]. TRDN is located in the SR of triad and dyad junctions in skeletal and cardiac muscles, where it communicates the status of calcium store filling to Ca^{2+} release via interactions with RyRs and CASQ [45]. TRDN can be found in several isoforms generated by alternate mRNA splicing, of 95 kDa and 51 kDa (Trisk95 and Trisk 51) in skeletal muscle and of 32 kDa (Trisk32), present mainly in heart [46]. The co-expression of a 95 kDa form of TRDN, together with CASQ, RyR1 and RyR3 suggests that the Ry-sensitive calcium release complex in trophoblasts is analogous to that in skeletal muscle. In addition to muscle cells and trophoblasts, the presence of CASQs has also been reported in chicken Purkinje neurons [44], zebrafish brain [47] and human oocytes [48]. This restricted cell-type distribution is suggestive of specialized roles of CASQs in Ca^{2+}-storage and signalling. Furthermore, to our knowledge, this is the first report of the presence of TRDN in a non-excitable cell-type and highlights the specialization of Ca^{2+} signalling in trophoblasts.

The data presented here indicate that the RyRs present in the BeWo cell-line form functional calcium channels. The rise in cytoplasmic Ca^{2+} triggered by 1 μM Ry could be partially inhibited by the local anaesthetic Tet. The effects of Tet were similar to those reported in heart and skeletal muscle fibres: an initial inhibition of the effects of Ry, followed by delayed Ca^{2+} release. The later phase of this response is considered to be due to Ca^{2+} levels within the ER surpassing a threshold, leading to store-overload-induced Ca^{2+}release [38]. Attempts to inhibit Ry-induced Ca^{2+}release using the RyR1/RyR3 antagonist dantrolene were unsuccessful, owing to the increase in autofluorescence at an excitation wavelength of 380 nm. Similar increases in autofluorescence at an excitation wavelength of 380 nm have been reported in bullfrog sympathetic neurons [39], but have not been consistently observed between different cell types. This suggests that trophoblastic cells and bullfrog sympathetic neurons contain a specific cellular component that promotes such autofluorescence. As alternatives, 100 μM concentration of Ry or Tet were reliable antagonists of RyR-mediated Ca^{2+} increases in trophoblasts.

AGII, AVP and ET1 increased $[Ca^{2+}]_c$ in the BeWo cell-line, via signalling pathways involving their cognate G-protein coupled receptors (AT1R, V1aR and ET_AR, respectively) and RyRs. The mechanisms by which G-protein coupled receptors could elicit RyR-dependent Ca^{2+} release were not resolved. The most probable pathway is amplification of Ca^{2+} release from IP_3R by CICR. Efforts to test this were unfruitful, since both the phospholipase C inhibitor U73122 and the IP_3R antagonist 2-APB elevated $[Ca^{2+}]_c$ in their own right. Published data indicate that U73122 can directly activate, rather than inhibit, certain phospholipase C isozymes [49]. Likewise, 2-APB can increase $[Ca^{2+}]_c$ by directly inhibiting SR/ER Ca^{2+}-ATPase pumps, leading to leakage of Ca^{2+} from intracellular stores [50] and can also directly gate the store-operated calcium entry channels Orai1 and Orai3 [51]. Future investigations to address this issue include expression of an engineered "IP_3 sponge" protein [52] in the BeWo cells (although these have proven difficult to transfect), or micro-injection of the membrane-impermeant IP_3R antagonist, low molecular weight heparin [53].

Coupling between receptors for peptide hormones and RyRs implies roles for these calcium release channels in regulation of the physiological activities of trophoblasts. Such cellular activities include inhibition of trophoblast invasion by AGII [21], stimulation of migration by ET1 in extravillous trophoblasts [54] and triggering of ER-stress in trophoblastic cell-lines [24]. The current work supports the notion that RyR-mediated Ca^{2+}-release modifies the migration of both BeWo and JEG-3 choriocarcinoma-derived cell-lines, by influencing the organization of the F-actin cytoskeleton. This might explain the presence of highly specialized Ca^{2+} release channels in trophoblasts. Due to their higher conductance and longer open duration, RyRs conduct about 25 times more Ca^{2+} per opening event than the IP_3Rs [55], they are more suited to generating large, transient and localized increases in Ca^{2+}. These are known as "Ca^{2+} sparks" and are produced through concerted opening of a small number of channel complexes. Such discrete Ca^{2+} release events could promote localized re-organization of the F-actin cytoskeleton, thereby contributing to cell motility [40], [56]. Decreased placental expression of RyRs in pathological states such as PE and intrauterine growth restriction [4] might contribute to impaired trophoblast migration.

Acknowledgements. This work was supported by funding from Science Foundation Ireland (Research Frontiers Project SFI/RFP2007/BMIF548 "Ryanodine Receptor expression in Trophoblasts") to JJM. We thank Dr. Tom Moore (UCC) for supplying term placental tissue and Prof. Berthold Huppertz (Medical University of Graz, Austria) for valuable discussions at the start of this project.

Figure legends

Figure 1. RyRs, triadin (TRDN) and calsequestrins (CASQ) are present in villous trophoblasts. The presence of **A.** RyR1, RyR2 and RyR3 and **B.** TRDN in human placental villous tissue sections was investigated by IHC microscopy (number of experiments, n = 3). *Panels A I, III, V, VII* and *IX* show representative micrographs of first trimester placentas, and *AII, IV, VI, VII* and *X* of term samples. The syncytiotrophoblast layer is indicated by '*'; and the cytotrophoblast layer by '▲', as verified by positive staining with anti-cytokeratin-7. 'Null' shows the staining pattern in the absence of primary antibodies. Scale-bar = 10 μm. **C. i)** TRDN is detected as a protein of 95 kDa apparent molecular weight in homogenates (80 μg protein/lane) from human term trimester (representative of n = 3) by mAb GE4.90. **ii)** Western immunoblot of term placental villi homogenates (80 μg protein/lane) with the polyclonal antibody recognizing CASQ. The positions of molecular weight markers are indicated on the left; positions of CASQs and CASQ-like proteins on the right.

Figure 2. Anti-RyR2 antiserum labels cells in the decidual bed of first trimester human placenta. RyR2 protein was detected by IHC microscopy in the decidual bed of first trimester tissue sections. **A.** The antiserum used recognizes RyR2. **B.** Negative control (no primary antibody); **C.** Positive staining for cytokeratin 7 indicates trophoblastic cells within the tissue section. These images are representative of three separate experiments. Scale-bar = 100 μm.

Figure 3. Detection of RyR1, RyR3, TRDN, CASQs and $Ca_V1.2/1.3$ voltage-gated Ca^{2+} channels in the BeWo choriocarcimoma.

A. Immunoblot assays indicate that RyR1 and RyR3 proteins are present in BeWo cells. Each lane contains microsomal protein (40 μg protein/lane) prepared from BeWo cells, or control cell-lines (A549, SH-SY5Y, MDA-MB-231) or rat tissue homogenates (10 μg protein/lane), previously reported to contain different RyR subtypes [8], [9]. The panel labelled 'IgG -ve control' was incubated with non-immune rabbit IgG at the same concentration used for the primary antibodies. The numbers of the left indicate the positions of molecular weight markers (HiMark prestained markers, ThermoFisher). Arrows indicate the positions of proteins migrating at appropriate molecular weight for RyRs (>500 kDa, as estimated from gel Rf values). Differences in migration between RyR1, RyR2 and RyR3 were anticipated from their calculated molecular weights. The asterix (*) indicates the migration of a protein non-specifically detected in the negative control experiment. **B.** Immunoblot of BeWo cell lysates (60 μg protein/lane) probed with antibodies recognising TRDN, CASQs or $Ca_V1.2/1.3$. Arrows

indicate the positions of major immunoreactive proteins. The numbers of the left indicate the positions of molecular weight markers.

Figure 4. Tetracaine (Tet) inhibits Ca^{2+} increases triggered by ryanodine (Ry) in BeWo cells. A. . Representative traces showing the effect of Ry (1 μM) in combination with Tet (100 μM) or vehicle (0.25% ethanol and 0.25% DMSO) when applied (arrow) to BeWo cells. **B.** Summary histogram of the increases in fura-2 ratio elicited by Ry (n =11), Ry + Tet (n = 8), or vehicle alone (n =3). These increases represent the difference between the mean resting fura-2 ratio (initial 1 min) and the peak value at any point following addition of reagents (subsequent 7 min). Statistical comparisons were made using ANOVA with Tukey's post-test; *a*, $p < 0.001$ versus vehicle; *b*, $p < 0.01$ versus Ry.

Figure 5. Effects of hormones, with or without their antagonists or RyR inhibitors, on $[Ca^{2+}]_c$ in Bewo cells. In all experiments, arrows indicate addition of peptide hormones and the bar-charts report maximal increases in fura-2 ratio following these additions. **A.** Fura-2 loaded BeWo cells were stimulated with 200 nM AGII in the presence or absence of 5 μM of the *Mas*R antagonist A779, 5 μM of the AT1R antagonist lorsartan, the RyR antagonists 100 μM Tet or 100 μM Ry, or with vehicle alone. The arrow indicates the time of addition of AGII. **B.** Bar-chart summarizing the effects of AGII (n = 9), AGII plus A779 (n = 5), AGII plus lorsartan (n = 3), AGII plus Ry (n = 5), AGII plus Tet (n= 3) or vehicle (n = 5) on rises in fura-2 ratio in BeWo cells (*a*, $p < 0.01$ *versus* vehicle; *b*, $p < 0.05$ *versus* AGII). **C.** Representative traces showing the effect of 200 nM AVP in the presence or absence of 100 nM SR49059, a V1aR selective antagonist, 100 μM Tet or 100 μM Ry, on BeWo $[Ca^{2+}]_c$. **D.** Bar-chart summarizing the mean increases in fura-2 ratio elicited by AVP (n = 6), AVP plus SR49059 (n = 4), AVP plus Ry (n = 5), AVP plus Tet (n = 5), or vehicle alone (n = 5) (*c*, $p < 0.05$ *versus* vehicle; *d*, $p < 0.01$ *versus* AVP). **E.** Representative traces showing the effect of 1 nM ET1 in the presence or absence of 100 nM BQ123, an ET_AR selective antagonist; 100 μM Tet or 100 μM Ry, or of vehicle alone, on fura-2 ratio in BeWo cells. **F.** Bar-chart summarizing rises in fura-2 ratio induced by ET1 (n = 6), ET1 plus BQ123 (n = 4), ET1 plus Ry (n = 5), ET1 plus Tet (n = 5) or vehicle (n =5) (*e*, $p < 0.01$ *versus* vehicle; *f*, $p < 0.01$ *versus* ET1, *g*, $p < 0.05$).

Figure 6. In BeWo cells, pretreatment with 100 μM Ry or 100 μM Tet does not deplete thapsigargin-sensitive Ca^{2+} stores. A. Fura-2 loaded BeWo cells were treated with either vehicle (V), 100 μM Ry (100Ry) or 100 μM Tet (Tet) for 5 min, then resting fura-2 ratios were recorded. Thapsigargin (500 nM, *arrow*) was then added and changes in fura-2 ratio monitored

for another 10 min, in the continued presence of V, 100Ry or Tet. **B.** Bar-chart summarizing changes in resting fura-2 ratio initiated by V (n = 5), 100 Ry (n = 6) or Tet (n = 7). The *p*-values shown indicate statistical differences between experimental groups, as determined by ANOVA. **C.** Bar-chart summarizing the effects of pre-treatment with V, 100 Ry, or Tet on the magnitude of the rise in fura-2 ratio in BeWo cells following addition of 500 nM TG. Pre-treatments were performed for either 5 min (n = 5, 6, or 7 for V, 100 Ry or Tet, respectively) or 8 h (n = 6 for all). Transients were estimated from AUC measured for 10 min after TG addition. Differences in these AUCs were not statistically significant ($p > 0.05$).

Figure 7. Inhibition of RyRs alters AGII stimulated changes in random migration by the BeWo choriocarcinoma. A. Representative plot of BeWo migration paths, in cells stimulated with 200 nM AGII for 8 h. **B.** Representative plot of migration paths, in BeWo cells stimulated with 200 nM AGII plus 100 μM Ry for 8 h. **C.** Bar-chart summarizing the effect of vehicle (V, n = 9), 100Ry alone (n = 9), AGII alone (n = 9) or AGII plus 100 Ry (n = 6) on the velocity of random migration. Statistical differences between groups were determined using ANOVA: *, p <0.05; ** p <0.01 *versus* AGII. **D.** Bar-chart summarizing the effect of these interventions on accumulated distance travelled. **E.** Bar-chart summarizing the effect of the manipulations on Euclidean distance travelled (***, p <0.001 *versus* AGII). **F.** Bar-chart summarizing the effect of V, 100Ry, AGII, or AGII plus 100Ry on the directionality of random migration in BeWo cells. Note that all additions significantly increased directionality compared with cells treated with vehicle alone (++, p <0.01; +++, p <0.001 *versus* V). **G.** Bar-chart summarizing the effect of vehicle (V, n = 4), Tet alone (n = 5), AGII alone (n = 9) or AGII plus Tet (n = 5) on the velocity of random migration. Statistical differences between groups were determined by ANOVA: *, p <0.05; ** p <0.01 *versus* AGII. **H.** Bar-chart summarizing the effect of Tet on accumulated distance travelled. Note that the mean values shown are approximately a quarter of those shown in panel **D**, because migration was recorded for 2 hours rather than 8 hours.

Figure 8. Changes in F-actin organization elicited by AGII in BeWo cells are abolished by inhibition of RyRs. A. Generation of data on F-actin organization. BeWo cells were incubated with V, 100Ry, AGII, or AGII plus Ry for 2 h, then were fixed, permeabilized and stained with Texas Red-phalloidin (for F-actin) and DAPI (DNA stain). **i)** Representative confocal micrograph of BeWo cells stained with Texas Red-phalloidin and DAPI; **ii)** the isolated Texas Red channel, with a region-of-interest drawn to select one cell. This allows calculation of the area of each cell and its orientation relative to the field of view; **iii)**

skeletonization ("simplification") of the F-actin staining; and **iv)** isolation of the cell of interest, by filling the background, to allow extraction of data on F-actin orientation (average angle to longest axis of the cell, length, density, parallelness and bundling). **B.** Bar-chart representing the effect of V, 100Ry, AGII, AGII plus Ry, Tet or AGII plus Tet on F-actin parallelness. Statistical significant differences between groups were identified by ANOVA and Tukey's post-hoc tests (for V, ***a***, $p < 0.01$ vs 100 Ry, ***b***, $p < 0.001$ vs AGII; for 100 Ry, ***c***, $p < 0.01$ vs 100 AGII + Tet, ***d***, $p < 0.001$ vs Tet; for AGII, ***e***, $p < 0.05$ vs AGII + 100 Ry, ***f***, $p < 0.001$ vs Tet, ***g***, $p < 0.001$ vs AGII + Tet; and ***h***, for AGII + 100 Ry,$p < 0.01$ vs Tet) . These data each represent the average of three experiments, each containing three technical replicates from three biological replicates and measurement of 5 cells from each (135 cells in total for each experiment).

References

[1] M. Hemberger, C. W. Hanna, and W. Dean, "Mechanisms of early placental development in mouse and humans," *Nat. Rev. Genet.*, vol. 21, no. 1, pp. 27–43, Jan. 2020, doi: 10.1038/s41576-019-0169-4.

[2] L. Belkacemi, I. Bédard, L. Simoneau, and J. Lafond, "Calcium channels, transporters and exchangers in placenta: a review," *Cell Calcium*, vol. 37, no. 1, pp. 1–8, Jan. 2005, doi: 10.1016/j.ceca.2004.06.010.

[3] R. Moreau, G. Daoud, A. Masse, L. Simoneau, and J. Lafond, "Expression and role of calcium-ATPase pump and sodium-calcium exchanger in differentiated trophoblasts from human term placenta," *Mol. Reprod. Dev.*, vol. 65, no. 3, pp. 283–288, Jul. 2003, doi: 10.1002/mrd.10303.

[4] S. Haché *et al.*, "Alteration of calcium homeostasis in primary preeclamptic syncytiotrophoblasts: effect on calcium exchange in placenta," *J. Cell. Mol. Med.*, vol. 15, no. 3, pp. 654–667, Mar. 2011, doi: 10.1111/j.1582-4934.2010.01039.x.

[5] M. J. Berridge, M. D. Bootman, and H. L. Roderick, "Calcium signalling: dynamics, homeostasis and remodelling," *Nat. Rev. Mol. Cell Biol.*, vol. 4, no. 7, pp. 517–529, Jul. 2003, doi: 10.1038/nrm1155.

[6] G. Meissner, "The structural basis of ryanodine receptor ion channel function," *J. Gen. Physiol.*, vol. 149, no. 12, pp. 1065–1089, Dec. 2017, doi: 10.1085/jgp.201711878.

[7] J. J. Mackrill, "Ryanodine receptor calcium channels and their partners as drug targets," *Biochem. Pharmacol.*, vol. 79, no. 11, pp. 1535–1543, Jun. 2010, doi: 10.1016/j.bcp.2010.01.014.

[8] G. Giannini, A. Conti, S. Mammarella, M. Scrobogna, and V. Sorrentino, "The ryanodine receptor/calcium channel genes are widely and differentially expressed in murine brain and peripheral tissues," *J. Cell Biol.*, vol. 128, no. 5, pp. 893–904, Mar. 1995, doi: 10.1083/jcb.128.5.893.

[9] J. J. Mackrill, R. A. Challiss, D. A. O'connell, F. A. Lai, and S. R. Nahorski, "Differential expression and regulation of ryanodine receptor and myo-inositol 1,4,5-trisphosphate receptor Ca2+ release channels in mammalian tissues and cell lines," *Biochem. J.*, vol. 327 (Pt 1), pp. 251–258, Oct. 1997, doi: 10.1042/bj3270251.

[10] H. Takeshima *et al.*, "Excitation-contraction uncoupling and muscular degeneration in mice lacking functional skeletal muscle ryanodine-receptor gene," *Nature*, vol. 369, no. 6481, pp. 556–559, Jun. 1994, doi: 10.1038/369556a0.

[11] E. Ríos, "Calcium-induced release of calcium in muscle: 50 years of work and the emerging consensus," *J. Gen. Physiol.*, vol. 150, no. 4, pp. 521–537, Apr. 2018, doi: 10.1085/jgp.201711959.

[12] H. Takeshima, S. Komazaki, K. Hirose, M. Nishi, T. Noda, and M. Iino, "Embryonic lethality and abnormal cardiac myocytes in mice lacking ryanodine receptor type 2," *EMBO J.*, vol. 17, no. 12, pp. 3309–3316, Jun. 1998, doi: 10.1093/emboj/17.12.3309.

[13] H. Takeshima *et al.*, "Generation and characterization of mutant mice lacking ryanodine receptor type 3," *J. Biol. Chem.*, vol. 271, no. 33, pp. 19649–19652, Aug. 1996, doi: 10.1074/jbc.271.33.19649.

[14] D. Rossi, A. Gamberucci, E. Pierantozzi, C. Amato, L. Migliore, and V. Sorrentino, "Calsequestrin, a key protein in striated muscle health and disease," *J. Muscle Res. Cell Motil.*, Jun. 2020, doi: 10.1007/s10974-020-09583-6.

[15] I. Marty, "Triadin regulation of the ryanodine receptor complex," *J. Physiol.*, vol. 593, no. 15, pp. 3261–3266, Aug. 2015, doi: 10.1113/jphysiol.2014.281147.

[16] C. Wei, X. Wang, M. Zheng, and H. Cheng, "Calcium gradients underlying cell migration," *Curr. Opin. Cell Biol.*, vol. 24, no. 2, pp. 254–261, Apr. 2012, doi: 10.1016/j.ceb.2011.12.002.

[17] M. Matyash, V. Matyash, C. Nolte, V. Sorrentino, and H. Kettenmann, "Requirement of functional ryanodine receptor type 3 for astrocyte migration," *FASEB J. Off. Publ. Fed. Am. Soc. Exp. Biol.*, vol. 16, no. 1, pp. 84–86, Jan. 2002, doi: 10.1096/fj.01-0380fje.

[18] J.-P. Chen, Y. Luan, C.-X. You, X.-H. Chen, R.-C. Luo, and R. Li, "TRPM7 regulates the migration of human nasopharyngeal carcinoma cell by mediating Ca(2+) influx," *Cell Calcium*, vol. 47, no. 5, pp. 425–432, May 2010, doi: 10.1016/j.ceca.2010.03.003.

[19] S. Carpi *et al.*, "Anticancer Activity of Euplotin C, Isolated from the Marine Ciliate Euplotes crassus, Against Human Melanoma Cells," *Mar. Drugs*, vol. 16, no. 5, p. E166, May 2018, doi: 10.3390/md16050166.

[20] K. G. Pringle, M. A. Tadros, R. J. Callister, and E. R. Lumbers, "The expression and localization of the human placental prorenin/renin-angiotensin system throughout pregnancy: roles in trophoblast invasion and angiogenesis?," *Placenta*, vol. 32, no. 12, pp. 956–962, Dec. 2011, doi: 10.1016/j.placenta.2011.09.020.

[21] Y. Xia, H. Y. Wen, and R. E. Kellems, "Angiotensin II inhibits human trophoblast invasion through AT1 receptor activation," *J. Biol. Chem.*, vol. 277, no. 27, pp. 24601–24608, Jul. 2002, doi: 10.1074/jbc.M201369200.

[22] I. Koukoulas, J. Risvanis, R. Douglas-Denton, L. M. Burrell, K. M. Moritz, and E. M. Wintour, "Vasopressin receptor expression in the placenta," *Biol. Reprod.*, vol. 69, no. 2, pp. 679–686, Aug. 2003, doi: 10.1095/biolreprod.102.013458.

[23] M. Bilban *et al.*, "Differential regulation of endothelin secretion and endothelin receptor mRNA levels in JAR, JEG-3, and BeWo choriocarcinoma cell lines and in human trophoblasts, their nonmalignant counterpart," *Arch. Biochem. Biophys.*, vol. 382, no. 2, pp. 245–252, Oct. 2000, doi: 10.1006/abbi.2000.2016.

[24] A. Jain, M. Olovsson, G. J. Burton, and H. Yung, "Endothelin-1 induces endoplasmic reticulum stress by activating the PLC-IP(3) pathway: implications for placental pathophysiology in preeclampsia," *Am. J. Pathol.*, vol. 180, no. 6, pp. 2309–2320, Jun. 2012, doi: 10.1016/j.ajpath.2012.03.005.

[25] C. Niger, A. Malassiné, and L. Cronier, "Calcium channels activated by endothelin-1 in human trophoblast," *J. Physiol.*, vol. 561, no. Pt 2, pp. 449–458, Dec. 2004, doi: 10.1113/jphysiol.2004.073023.

[26] J. Mouton, I. Marty, M. Villaz, A. Feltz, and Y. Maulet, "Molecular interaction of dihydropyridine receptors with type-1 ryanodine receptors in rat brain," *Biochem. J.*, vol. 354, no. Pt 3, pp. 597–603, Mar. 2001, doi: 10.1042/0264-6021:3540597.

[27] K. Forbes, M. Westwood, P. N. Baker, and J. D. Aplin, "Insulin-like growth factor I and II regulate the life cycle of trophoblast in the developing human placenta," *Am. J. Physiol. Cell Physiol.*, vol. 294, no. 6, pp. C1313-1322, Jun. 2008, doi: 10.1152/ajpcell.00035.2008.

[28] R. A. Pattillo, G. O. Gey, E. Delfs, and R. F. Mattingly, "Human hormone production in vitro," *Science*, vol. 159, no. 3822, pp. 1467–1469, Mar. 1968, doi: 10.1126/science.159.3822.1467.

[29] Z. Mahdy, H. A. Otun, W. Dunlop, and J. I. Gillespie, "The responsiveness of isolated human hand vein endothelial cells in normal pregnancy and in pre-eclampsia," *J. Physiol.*, vol. 508 (Pt 2), pp. 609–617, Apr. 1998, doi: 10.1111/j.1469-7793.1998.00609.x.

[30] O. Thastrup, P. J. Cullen, B. K. Drøbak, M. R. Hanley, and A. P. Dawson, "Thapsigargin, a tumor promoter, discharges intracellular Ca2+ stores by specific inhibition of the endoplasmic reticulum Ca2(+)-ATPase," *Proc. Natl. Acad. Sci. U. S. A.*, vol. 87, no. 7, pp. 2466–2470, Apr. 1990, doi: 10.1073/pnas.87.7.2466.

[31] F. O. Lemos, G. Bultynck, and J. B. Parys, "A comprehensive overview of the complex world of the endo- and sarcoplasmic reticulum Ca2+-leak channels," *Biochim. Biophys. Acta Mol. Cell Res.*, vol. 1868, no. 7, p. 119020, Jun. 2021, doi: 10.1016/j.bbamcr.2021.119020.

[32] V. Semmling *et al.*, "Alternative cross-priming through CCL17-CCR4-mediated attraction of CTLs toward NKT cell-licensed DCs," *Nat. Immunol.*, vol. 11, no. 4, pp. 313–320, Apr. 2010, doi: 10.1038/ni.1848.

[33] T. Higaki, "Quantitative evaluation of cytoskeletal organizations by microscopic image analysis," *PLANT Morphol.*, vol. 29, no. 1, pp. 15–21, 2017, doi: 10.5685/plmorphol.29.15.
[34] I. Damjanov, M. Osborn, and M. Miettinen, "Keratin 7 is a marker for a subset of trophoblastic cells in human germ cell tumors," *Arch. Pathol. Lab. Med.*, vol. 114, no. 1, pp. 81–83, Jan. 1990.
[35] H. Fan, N. R. Brandt, and A. H. Caswell, "Disulfide bonds, N-glycosylation and transmembrane topology of skeletal muscle triadin," *Biochemistry*, vol. 34, no. 45, pp. 14902–14908, Nov. 1995, doi: 10.1021/bi00045a035.
[36] S. E. Cala and L. R. Jones, "Rapid purification of calsequestrin from cardiac and skeletal muscle sarcoplasmic reticulum vesicles by Ca2+-dependent elution from phenyl-sepharose," *J. Biol. Chem.*, vol. 258, no. 19, pp. 11932–11936, Oct. 1983.
[37] K. Culligan, N. Banville, P. Dowling, and K. Ohlendieck, "Drastic reduction of calsequestrin-like proteins and impaired calcium binding in dystrophic mdx muscle," *J. Appl. Physiol. Bethesda Md 1985*, vol. 92, no. 2, pp. 435–445, Feb. 2002, doi: 10.1152/japplphysiol.00903.2001.
[38] L. Csernoch, P. Szentesi, S. Sárközi, C. Szegedi, I. Jona, and L. Kovács, "Effects of tetracaine on sarcoplasmic calcium release in mammalian skeletal muscle fibres," *J. Physiol.*, vol. 515 (Pt 3), pp. 843–857, Mar. 1999, doi: 10.1111/j.1469-7793.1999.843ab.x.
[39] M. Nohmi, K. Kuba, and S. Y. Hua, "Ultraviolet light activates blocking actions of dantrolene on intracellular Ca2+ release in bullfrog sympathetic neurones," *J. Biol. Chem.*, vol. 266, no. 33, pp. 22254–22259, Nov. 1991.
[40] J. Stricker, T. Falzone, and M. L. Gardel, "Mechanics of the F-actin cytoskeleton," *J. Biomech.*, vol. 43, no. 1, pp. 9–14, Jan. 2010, doi: 10.1016/j.jbiomech.2009.09.003.
[41] J. Riedl *et al.*, "Lifeact: a versatile marker to visualize F-actin," *Nat. Methods*, vol. 5, no. 7, pp. 605–607, Jul. 2008, doi: 10.1038/nmeth.1220.
[42] C. Silvin, B. Belisle, and A. Abo, "A role for Wiskott-Aldrich syndrome protein in T-cell receptor-mediated transcriptional activation independent of actin polymerization," *J. Biol. Chem.*, vol. 276, no. 24, pp. 21450–21457, Jun. 2001, doi: 10.1074/jbc.M010729200.
[43] M. J. Berridge, P. Lipp, and M. D. Bootman, "The versatility and universality of calcium signalling," *Nat. Rev. Mol. Cell Biol.*, vol. 1, no. 1, pp. 11–21, Oct. 2000, doi: 10.1038/35036035.
[44] A. Villa, P. Podini, D. O. Clegg, T. Pozzan, and J. Meldolesi, "Intracellular Ca2+ stores in chicken Purkinje neurons: differential distribution of the low affinity-high capacity Ca2+ binding protein, calsequestrin, of Ca2+ ATPase and of the ER lumenal protein, Bip," *J. Cell Biol.*, vol. 113, no. 4, pp. 779–791, May 1991, doi: 10.1083/jcb.113.4.779.
[45] C. M. Knudson, K. K. Stang, C. R. Moomaw, C. A. Slaughter, and K. P. Campbell, "Primary structure and topological analysis of a skeletal muscle-specific junctional sarcoplasmic reticulum glycoprotein (triadin)," *J. Biol. Chem.*, vol. 268, no. 17, pp. 12646–12654, Jun. 1993.
[46] M. Peng, H. Fan, T. L. Kirley, A. H. Caswell, and A. Schwartz, "Structural diversity of triadin in skeletal muscle and evidence of its existence in heart," *FEBS Lett.*, vol. 348, no. 1, pp. 17–20, Jul. 1994, doi: 10.1016/0014-5793(94)00556-7.
[47] S. Furlan *et al.*, "Calsequestrins New Calcium Store Markers of Adult Zebrafish Cerebellum and Optic Tectum," *Front. Neuroanat.*, vol. 14, p. 15, 2020, doi: 10.3389/fnana.2020.00015.
[48] H. Balakier, E. Dziak, A. Sojecki, C. Librach, M. Michalak, and M. Opas, "Calcium-binding proteins and calcium-release channels in human maturing oocytes, pronuclear zygotes and early preimplantation embryos," *Hum. Reprod. Oxf. Engl.*, vol. 17, no. 11, pp. 2938–2947, Nov. 2002, doi: 10.1093/humrep/17.11.2938.
[49] R. R. Klein *et al.*, "Direct activation of human phospholipase C by its well known inhibitor u73122," *J. Biol. Chem.*, vol. 286, no. 14, pp. 12407–12416, Apr. 2011, doi: 10.1074/jbc.M110.191783.
[50] J. G. Bilmen, L. L. Wootton, R. E. Godfrey, O. S. Smart, and F. Michelangeli, "Inhibition of SERCA Ca2+ pumps by 2-aminoethoxydiphenyl borate (2-APB). 2-APB reduces both Ca2+ binding and phosphoryl transfer from ATP, by interfering with the pathway leading to the Ca2+-binding

sites," *Eur. J. Biochem.*, vol. 269, no. 15, pp. 3678–3687, Aug. 2002, doi: 10.1046/j.1432-1033.2002.03060.x.

[51] W. I. DeHaven, J. T. Smyth, R. R. Boyles, G. S. Bird, and J. W. Putney, "Complex actions of 2-aminoethyldiphenyl borate on store-operated calcium entry," *J. Biol. Chem.*, vol. 283, no. 28, pp. 19265–19273, Jul. 2008, doi: 10.1074/jbc.M801535200.

[52] T. Uchiyama, F. Yoshikawa, A. Hishida, T. Furuichi, and K. Mikoshiba, "A novel recombinant hyperaffinity inositol 1,4,5-trisphosphate (IP(3)) absorbent traps IP(3), resulting in specific inhibition of IP(3)-mediated calcium signaling," *J. Biol. Chem.*, vol. 277, no. 10, pp. 8106–8113, Mar. 2002, doi: 10.1074/jbc.M108337200.

[53] L. C. Chopra, C. H. Twort, J. P. Ward, and I. R. Cameron, "Effects of heparin on inositol 1,4,5-trisphosphate and guanosine 5'-O-(3-thio triphosphate) induced calcium release in cultured smooth muscle cells from rabbit trachea," *Biochem. Biophys. Res. Commun.*, vol. 163, no. 1, pp. 262–268, Aug. 1989, doi: 10.1016/0006-291x(89)92130-x.

[54] C. Chakraborty, Y. P. Barbin, S. Chakrabarti, P. Chidiac, S. J. Dixon, and P. K. Lala, "Endothelin-1 promotes migration and induces elevation of [Ca2+]i and phosphorylation of MAP kinase of a human extravillous trophoblast cell line," *Mol. Cell. Endocrinol.*, vol. 201, no. 1–2, pp. 63–73, Mar. 2003, doi: 10.1016/s0303-7207(02)00431-8.

[55] B. E. Ehrlich, E. Kaftan, S. Bezprozvannaya, and I. Bezprozvanny, "The pharmacology of intracellular Ca(2+)-release channels," *Trends Pharmacol. Sci.*, vol. 15, no. 5, pp. 145–149, May 1994, doi: 10.1016/0165-6147(94)90074-4.

[56] F.-C. Tsai, G.-H. Kuo, S.-W. Chang, and P.-J. Tsai, "Ca2+ signaling in cytoskeletal reorganization, cell migration, and cancer metastasis," *BioMed Res. Int.*, vol. 2015, p. 409245, 2015, doi: 10.1155/2015/409245.

Figure 1

Click here to access/download;Figure;LZ BBA Fig 1.pptx

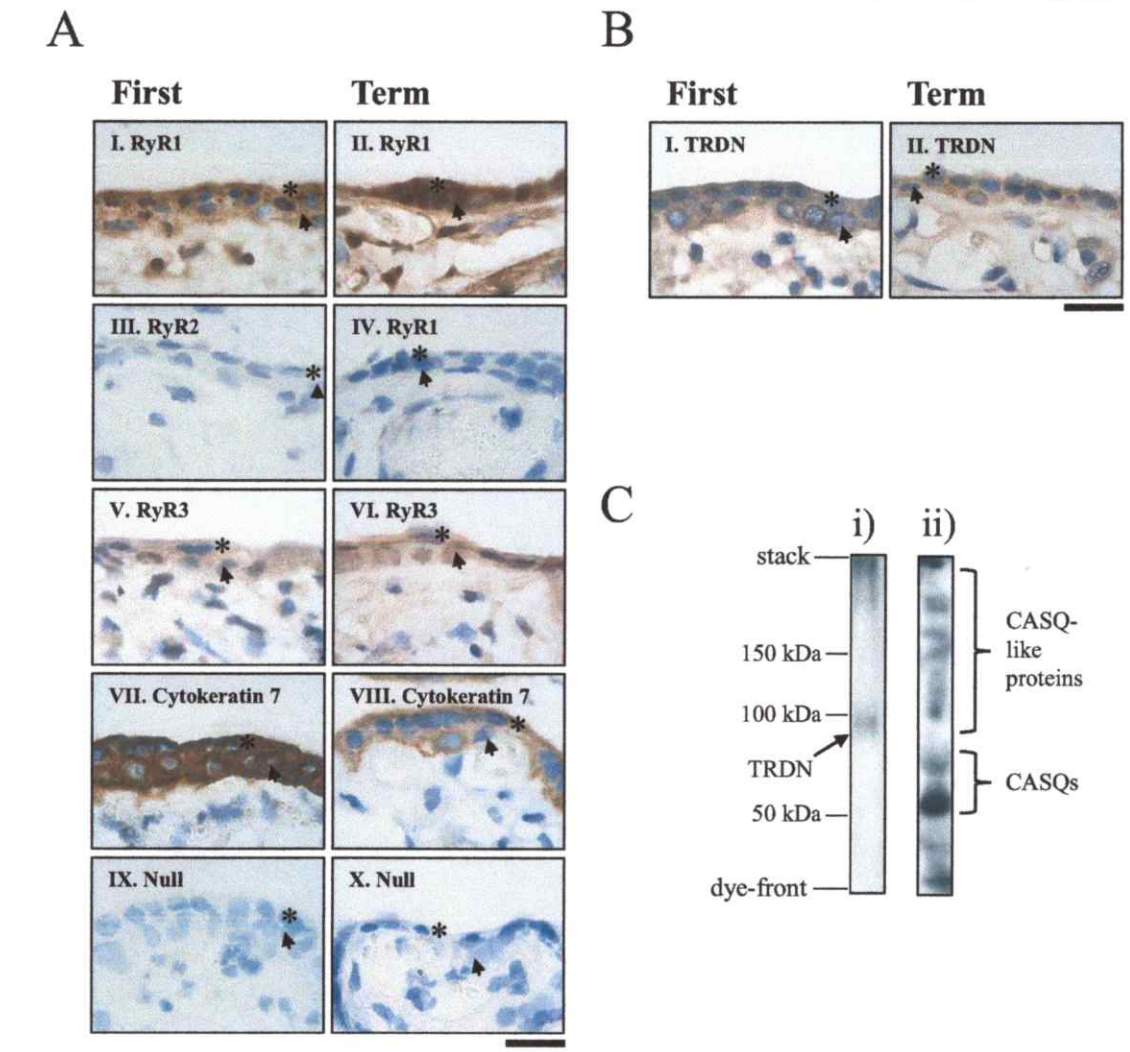

Figure 2

Click here to access/download;Figure;LZ BBA Fig 2.pptx

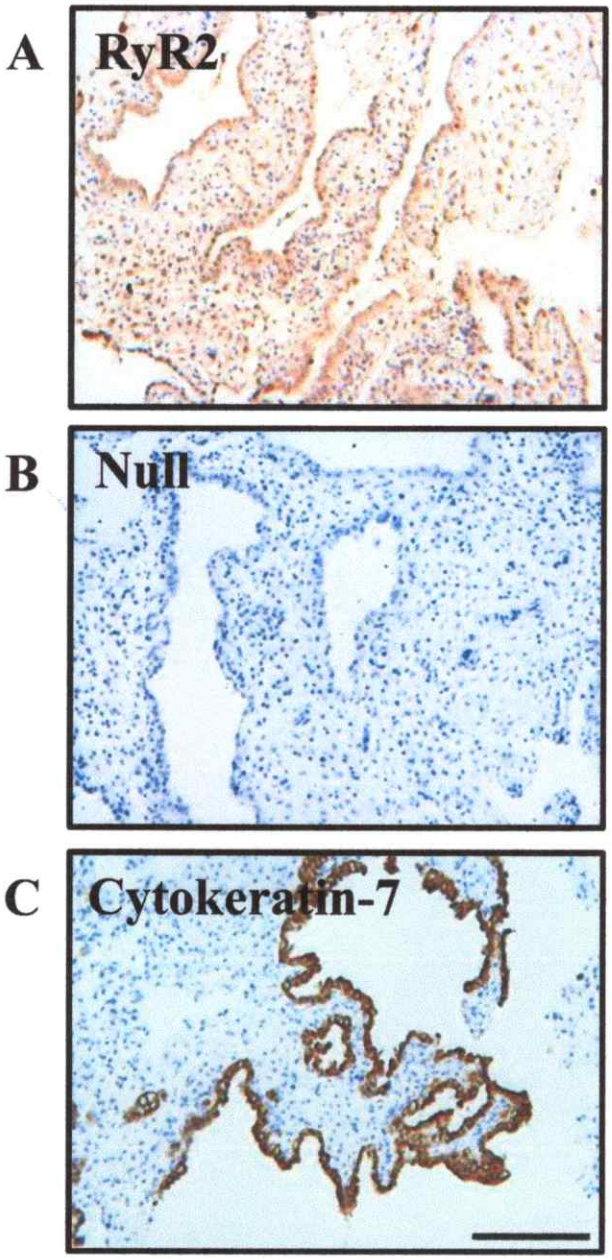

Figure 3

Click here to access/download;Figure;LZ BBA Fig 3 R1.pptx

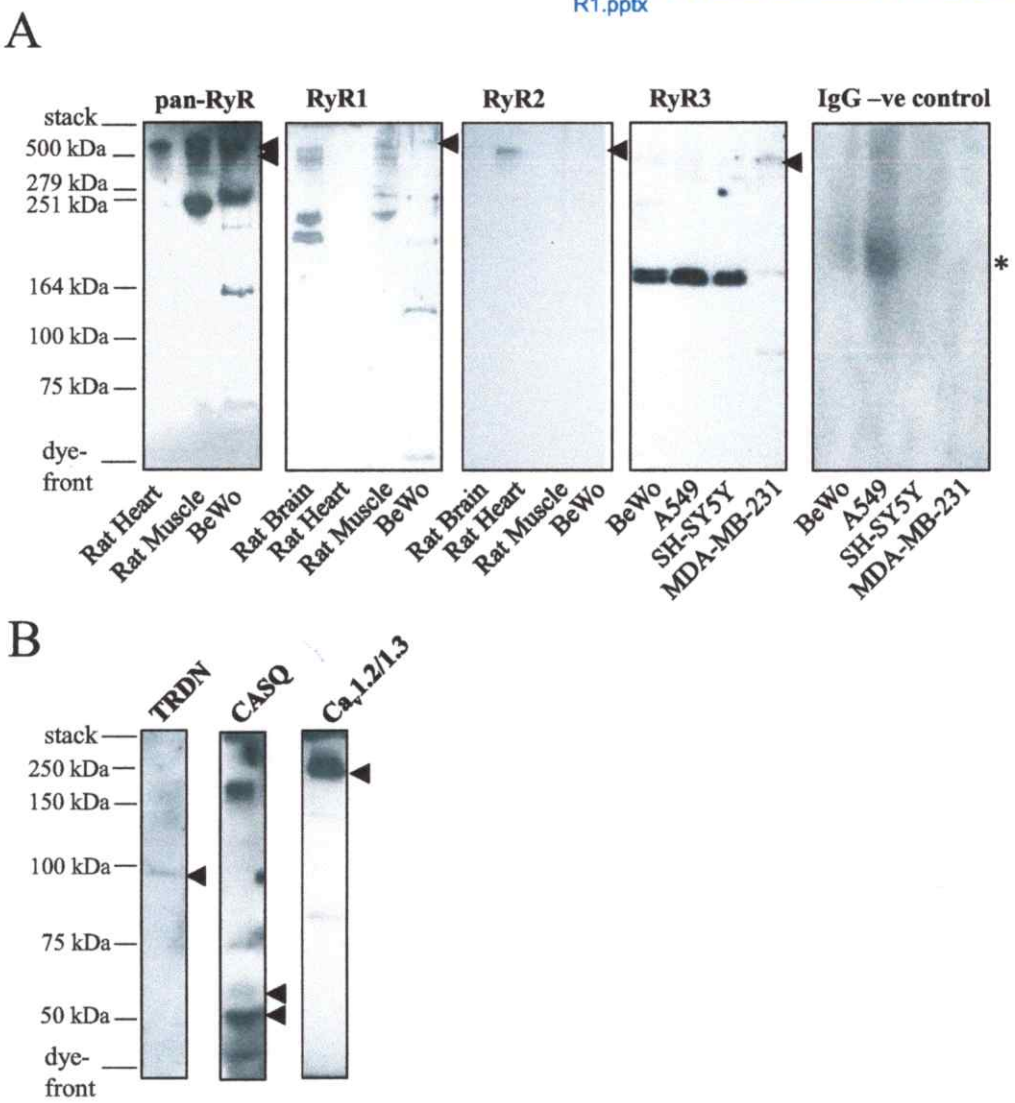

A

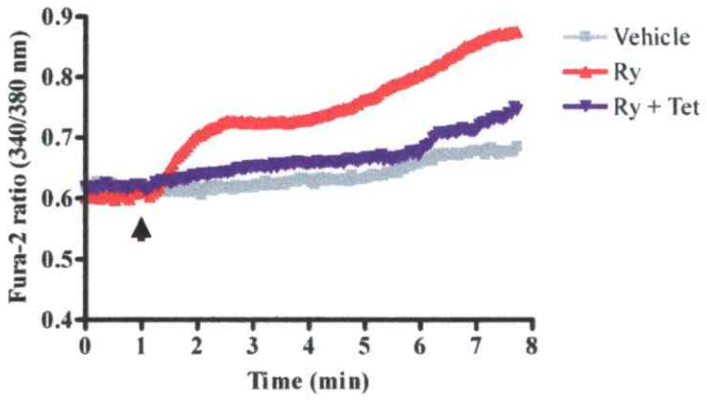

B

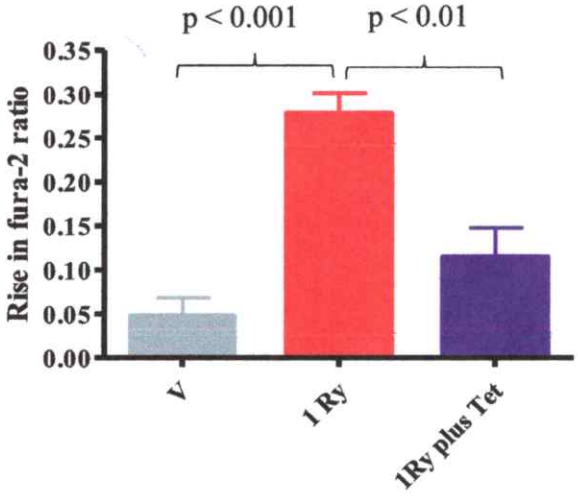

Figure 5

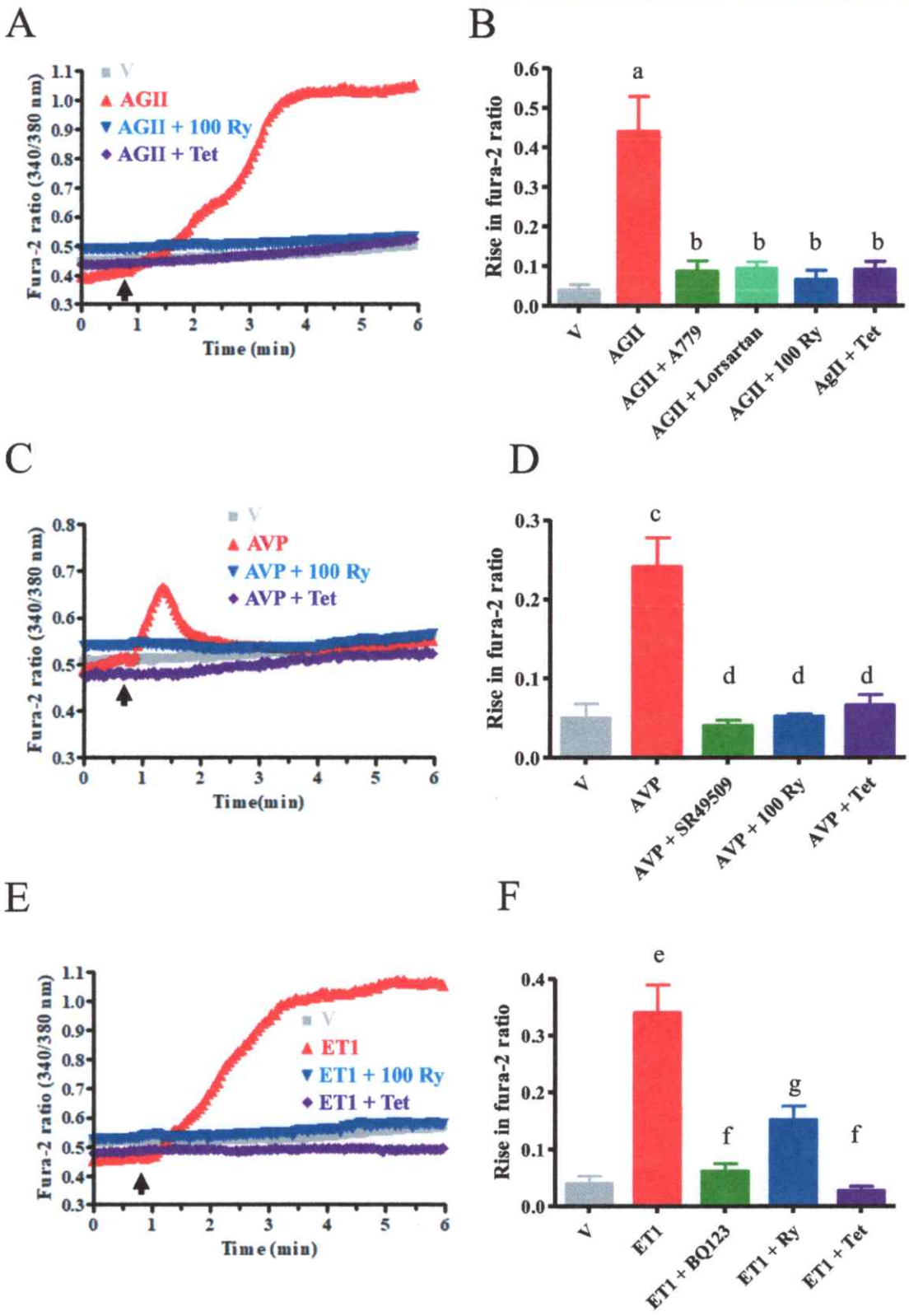

Figure 6

Click here to access/download;Figure;LZ BBA Fig 6 R1.pptx

A

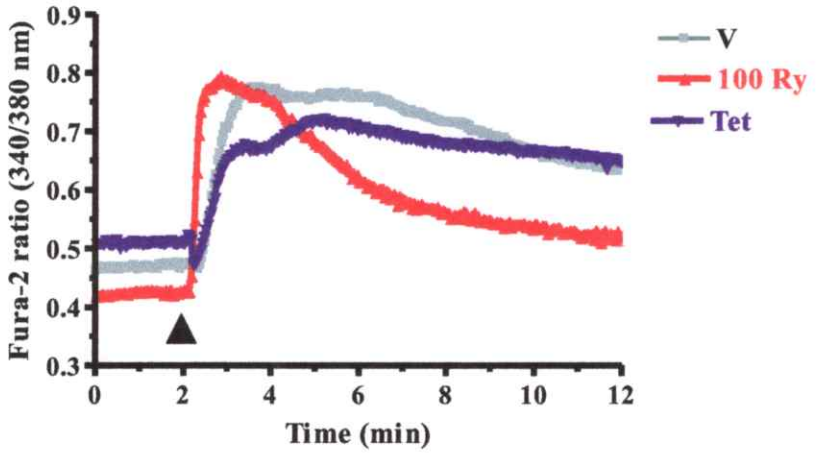

B

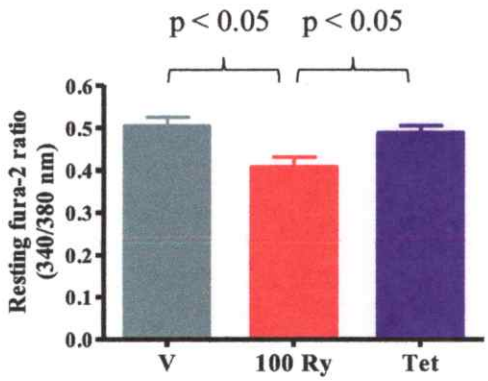

C

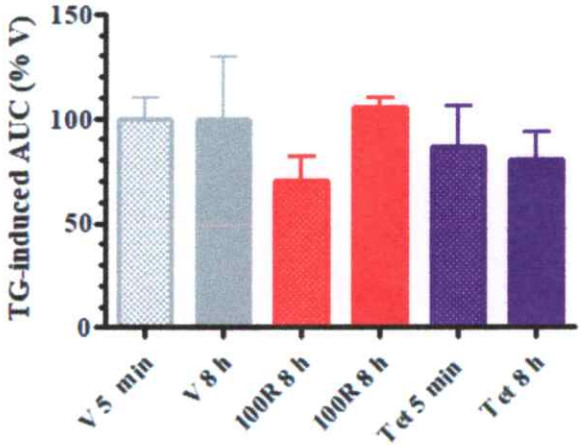

Figure 7

Click here to access/download;Figure;LZ BBA Fig 7.1.pptx

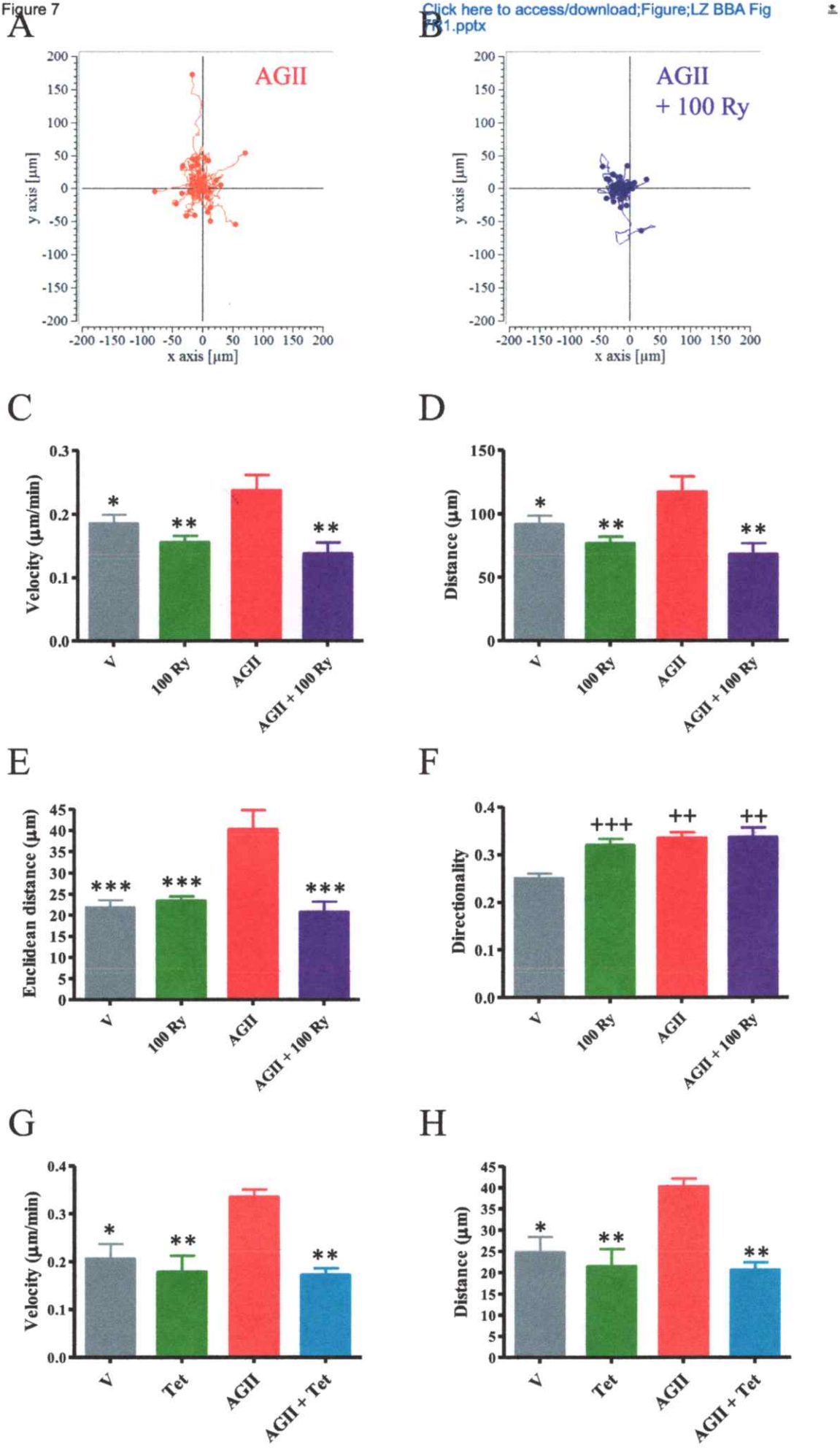

Figure 8

Click here to access/download;Figure;LZ BBA Fig 8 R1.pptx

A

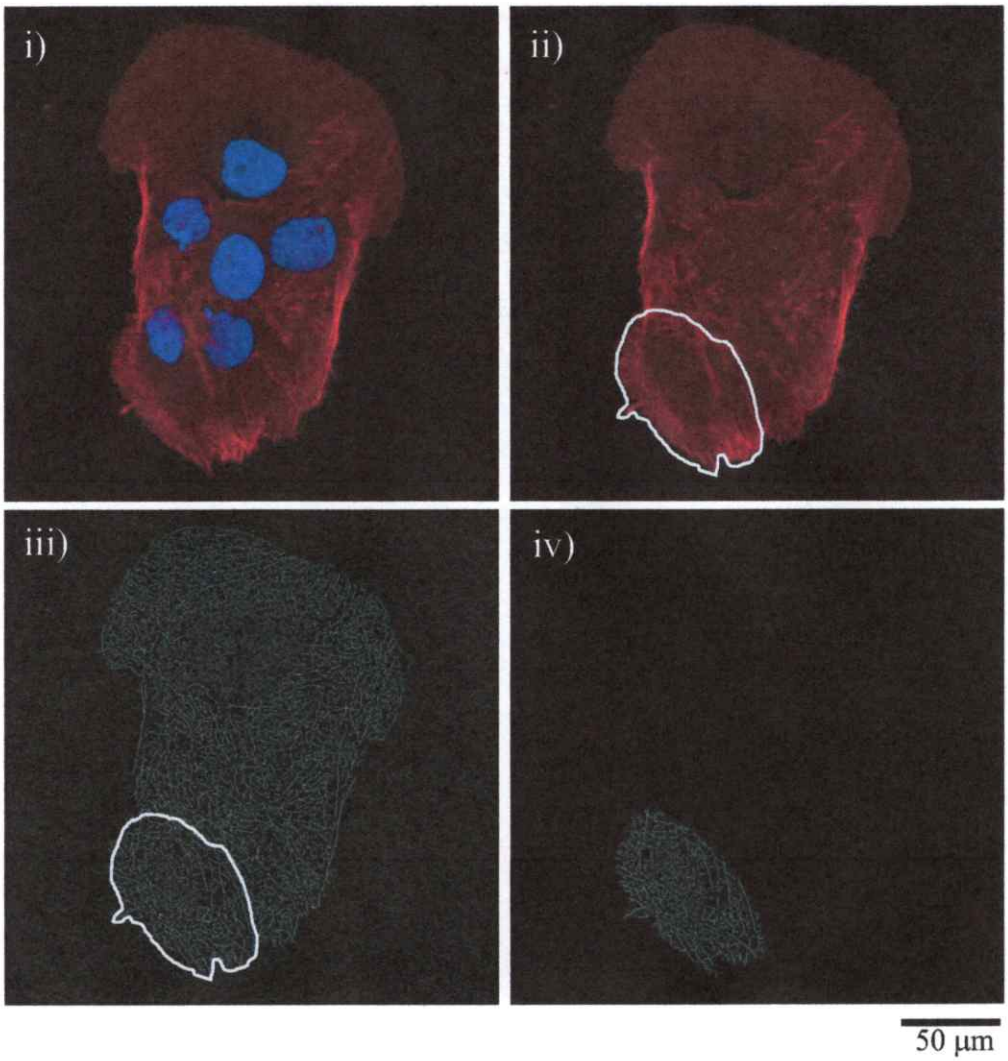

B

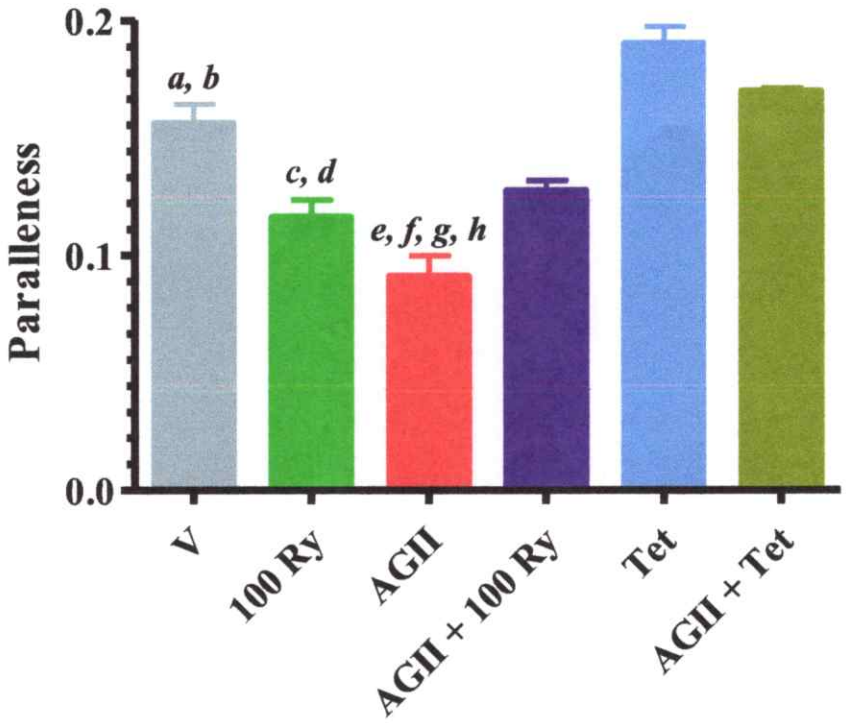

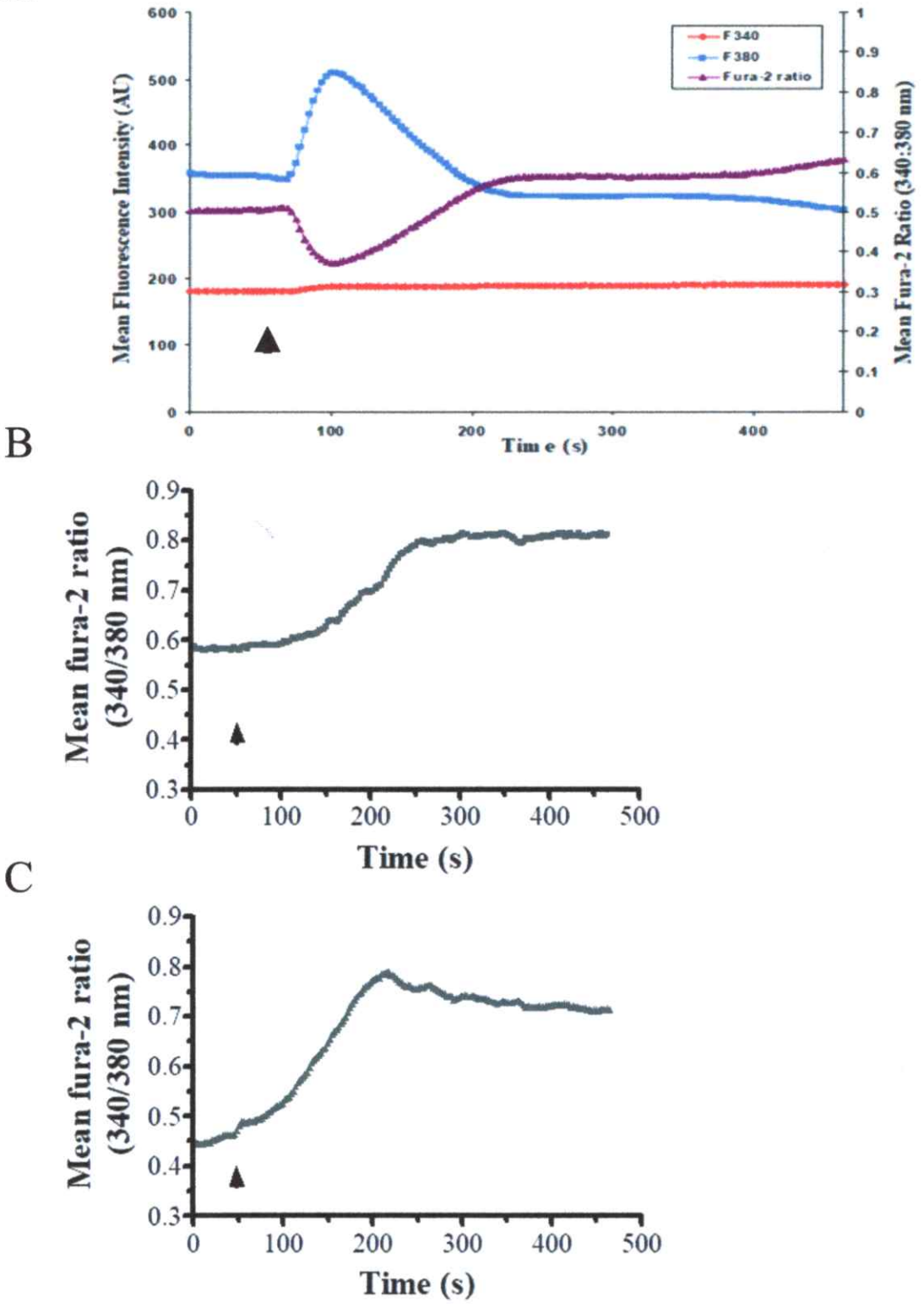

Supplemental Figure 2. Effects of Dantrolene, U73122 and 2-aminoethoxydiphenyl borate (2-APB) on Fura-2-loaded BeWo Cells. BeWo cells were loaded with fura-2 and imaged by fluorescent videomicroscopy, as described in the Material and Methods section. **A.** 50 μM dantrolene (an RyR antagonist, added at arrow) caused an artefactual rise in fluorescence emitted at an excitation wavelength of 380 nm. This effect was observed even in the absence of fura-2 and caused an artefactual decrease in the 340/380 nm ratio. In contrast, both **B** the phospholipase C inhibitor U73122 (1 μM, arrow) and **C** the IP_3R antagonist 2-APB (100 μM, arrow) caused increases in the 340/380 nm ratio of fura-2. These traces are representative of at least three independent experiments.

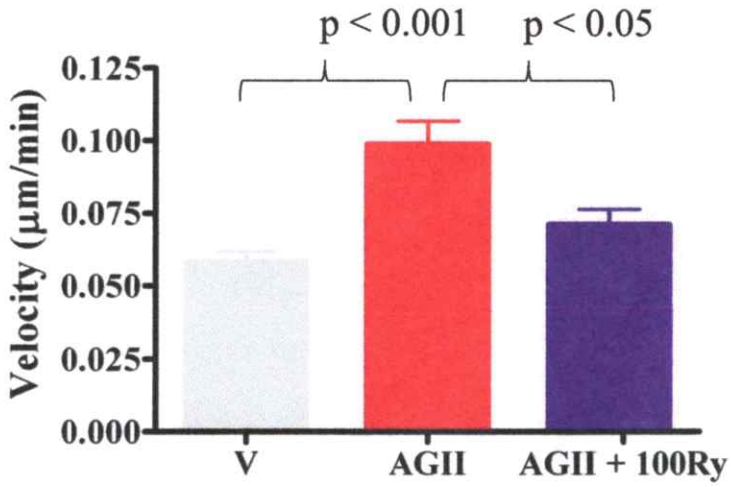

Supplemental Figure 2. Effects of 200 nM Angiotensin II (AGII), with or without 100 µM Ryanodine), on the Velocity of Migration of Human JEG-3 Trophoblastic Cells. These experiments were performed essentially as described for BeWo cells, Fig. 7 of main paper, and are display the mean values of at least five independent experiments. Error bars show the standard error of these mean values.

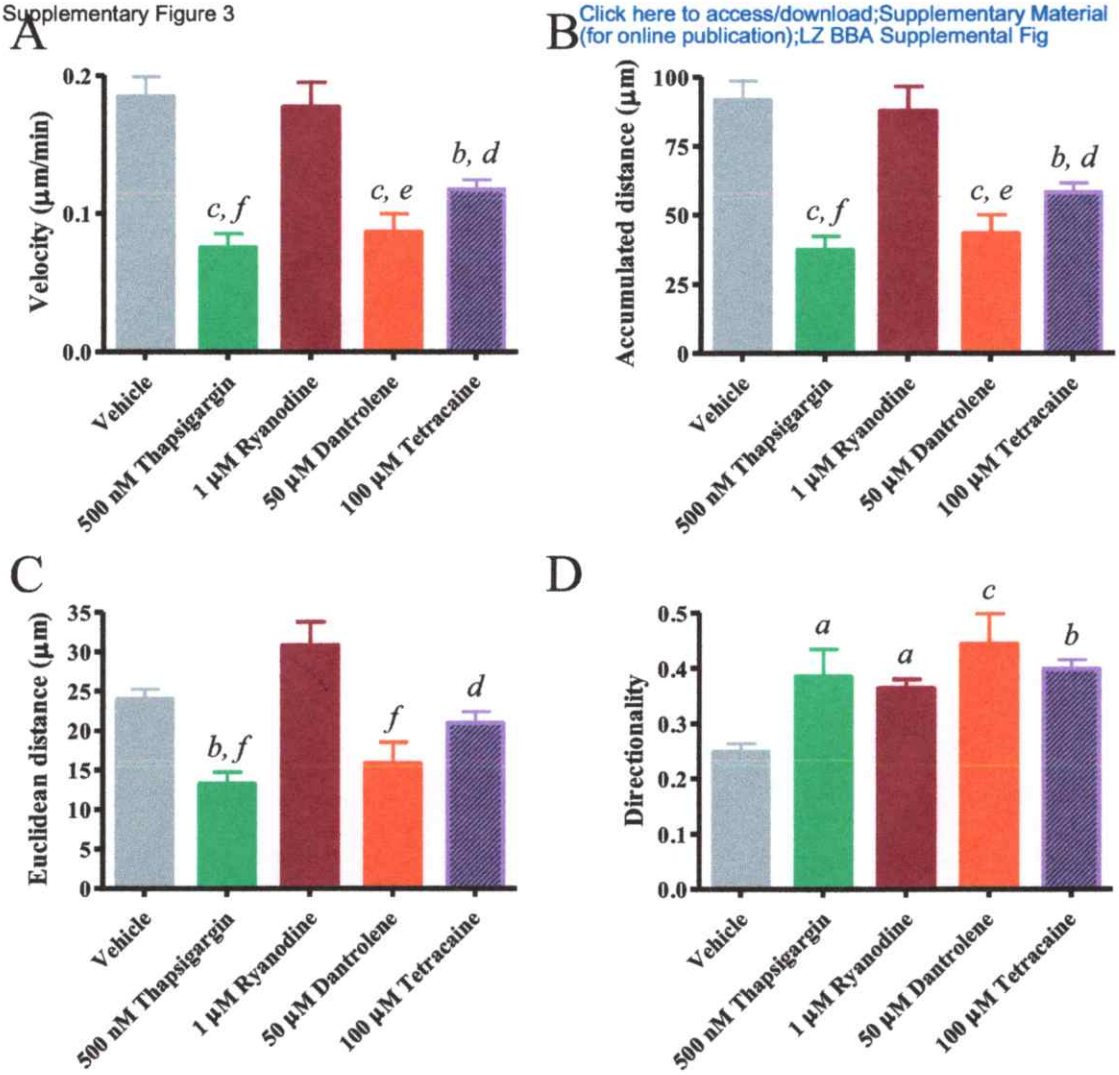

Supplemental Figure 3. Effects of Modifiers of ER Ca2+ Fluxes on BeWo Cell Migration. BeWo cells were treated with RyR antagonists (dantrolene and Tet), Ry at an agonistic concentration (1 µM), or the SERCA pump inhibitor thapsigargin and the effects on migration were monitored for 8 h. Panel **A** indicates cell velocity; **B** accumulated distance travelled; **C** Euclidean distance travelled; and **D** the directionality of migration. Solid bars represent the mean values of at least 5 separate experiments and error-bars, the standard error of these mean values. Statistical comparisons were made using ANOVA with Tukey's *post-hoc* test: *a*, $p < 0.05$, *b* <0.01 and *c* <0.001 versus Vehicle-treated cells; and *d*, $p < 0.05$, *e* <0.01 and *f* <0.001 versus cells treated with 1 µM Ry.

Supplementary Table 1

Click here to access/download;Supplementary Material (for online publication);LZ BBA Supplemental Table 1.xlsx

Supplemental Table 1. RyR protein types reported in rat tissues and human cell-lines

	RyR Type		
Tissue/Cell-line	RyR1	RyR2	RyR
Rat sk. Muscle	+++	-	+
Rat heart	-	+++	-
Rat brain	+	++	+
A549 cells	+	-	-
SH-SY5Y cells	-	+	-
MDA-MB-231	-	-	+

-	**undetected**
+	**low levels**
++	**medium**
+++	**high levels**

Supplementary Video 1

Click here to access/download
Supplementary Multimedia File
LZ BBA Supplemental Video 1.pptx

*Declaration of Interest Statement

Click here to access/download

Declaration of Interest Statement

BBA Zheng et al declaration-of-competing-interests.docx

Credit Author Statement

All authors contributed to aspects of experimental design, data acquisition, analysis and presentation; and to critical review of the manuscript. This work was conceptualized and managed by JJM. LZ and JJM performed the majority of Western blotting, Ca^{2+} imaging and cell migration experiments. Cell imaging experiments were also performed and analyzed by KM. RT developed several antibodies used in this project. AL designed and performed actin imaging experiments; these were analyzed by JJM. KF, SS and JA, designed, performed and analyzed IHC experiments, hosting LZ in their laboratory. JJM prepared the initial manuscript and generated revision. JJM also held the grant funding this research.